General Disclaimer

One or more of the Following Statements may affect this Document

- This document has been reproduced from the best copy furnished by the organizational source. It is being released in the interest of making available as much information as possible.

- This document may contain data, which exceeds the sheet parameters. It was furnished in this condition by the organizational source and is the best copy available.

- This document may contain tone-on-tone or color graphs, charts and/or pictures, which have been reproduced in black and white.

- This document is paginated as submitted by the original source.

- Portions of this document are not fully legible due to the historical nature of some of the material. However, it is the best reproduction available from the original submission.

Produced by the NASA Center for Aerospace Information (CASI)

FINAL REPORT

NASA RESEARCH GRANT NGR-22-011-007

INTER-RELATIONS BETWEEN ADVANCED PROCESSING TECHNIQUES, INTEGRATED CIRCUITS, MATERIALS DEVELOPMENT AND ANALYSIS

W. B. Nowak

B. L. Cochrun

W. Carlson

A. Grabel

FACILITY FORM 602

N71-37799 (ACCESSION NUMBER) — N71-37802 (THRU)

77 (PAGES) — 63 (CODE)

CR-123007 (NASA CR OR TMX OR AD NUMBER) — 10 (CATEGORY)

Northeastern University
Boston, Massachusetts

1 June 1971

OCT 1971
RECEIVED
NASA STI FACILITY
INPUT BRANCH

Reproduced by
NATIONAL TECHNICAL
INFORMATION SERVICE
Springfield, Va. 22151

N71-37799-802

INTER-RELATIONS BETWEEN ADVANCED PROCESSING TECHNIQUES, INTEGRATED CIRCUITS, MATERIALS DEVELOPMENT AND ANALYSIS

W. B. Nowak, et al

Northeastern University
Boston, Massachusetts

1 June 1971

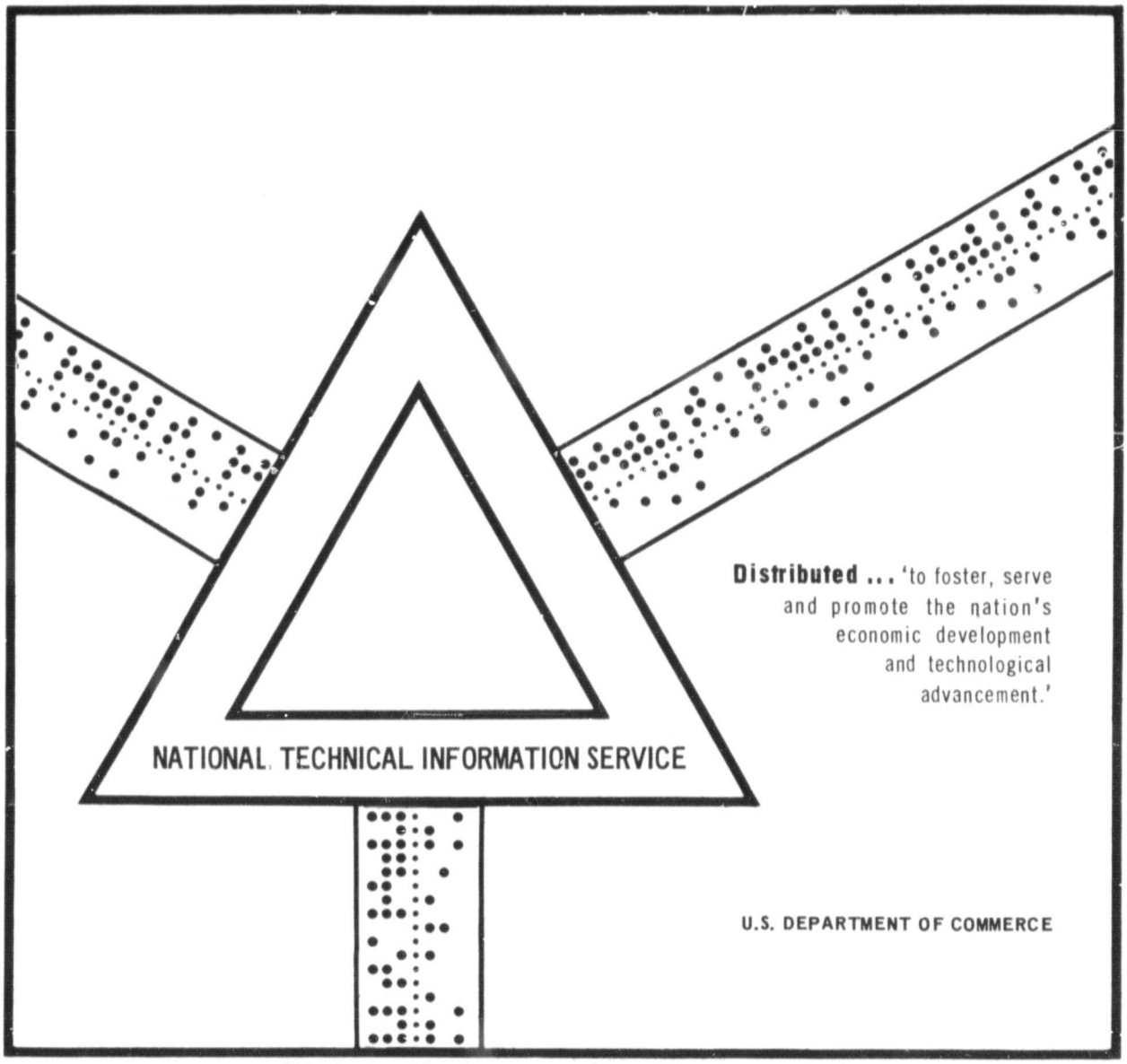

This document has been approved for public release and sale.

FINAL REPORT

NASA RESEARCH GRANT NGR-22-011-007

INTER-RELATIONS BETWEEN ADVANCED PROCESSING TECHNIQUES, INTEGRATED CIRCUITS, MATERIALS DEVELOPMENT AND ANALYSIS

W. B. Nowak
B. L. Cochrun
W. Carlson
A. Grabel

Northeastern University
Boston, Massachusetts

1 June 1971

The research reported here was sponsored by the National Aeronautics and Space Administration under Research Grant NGR-22-011-007 for the period from 30 November 1969 through 30 November 1970. This report is published for information purposes only and does not represent recommendations or conclusions of the sponsoring agency. Reproduction in whole or part is permitted for any purpose of the United States Government.

RESEARCH STAFF

Welville B. Nowak,	Co-principal Investigator Professor of Mechanical Engineering
Basil L. Cochrun,	Co-principal Investigator Professor of Electrical Engineering
Samuel Fine,	Professor Bio-Medical Engineering
Arvin Grabel,	Associate Professor of Electrical Engineering
William Carlson,	Engineer
D. MacKeen,	Graduate Student

TABLE OF CONTENTS

N71-37800

Section I

Active Integrated Circuits

B. L. Cochrun
W. Carlson
A. Grabel

Introduction

This section covers the investigation of gyrator applications as related to integrated circuits under NASA Grant NGR-22-011-007 from 1 December 1968 through 31 December 1970.

Attention has been given to the use of gyrators for tuned IF amplifiers with the development of a 455 kHz AM amplifier which would be suitable for integrated circuits. Consideration has also been given to the practical realization of a gyrator utilizing stable NIC configurations in cascade.

A. A Practical Tuned Amplifier Using Gyrators

A 455 kHz i.f. amplifier using gryator tuned circuits has been built. The amplifier has a 10 kHz bandwidth and a voltage gain of 2400.

The Sipress and Witt[1] gyrator, hereafter abbreviated to S-W gyrator, is used in the i.f. amplifier; the basic circuit of the S-W gyrator is shown in Figure 1. The circuit has the advantage of simplicity, and because Q_1 is used as an emitter follower the collector is available as an output by placing a resistor in series with the collector circuit while an input signal can be injected at a number of points in the circuit. The circuit can be used as a tuned amplifier by connecting a capacitor to each of the two parts.

The gyrator has a maximum Q[2, 3] of

$$Q_{max} \approx 1/2 \sqrt{\beta_1 \beta_2} .$$

If the Q is too high, it may be reduced by suitably loading one or both ports with shunt conductance. On the other hand, the Q of the basic S-W circuit may be less than desired, due to the gain of the transistors or to unavoidable losses

in biasing the circuit. The Q may be increased by modifying the S-W gyrator as shown in Figure 2[4]. Here the conductances G_{B1} and G_{B2} represent losses introduced by bias circuits. The modified circuit operates in this manner: with port two shorted, transistors Q_1 and Q_2 act as a negative reactance converter to convert G_4 to a negative conductance at port 1; similarly, with port 1 shorted, transistors Q_2 and Q_3 convert G_3 to a negative conductance at port 2. This is shown in the admittance matrix for the circuit given in Figure 2. The maximum Q of a practical gyrator is proportional to the square root of the ratio of the product of the gyrator conductances to the product of the input conductances, thus it is apparent that the Q may be increased by reducing y_{11} and y_{22} by means of G_4 and G_3 in the modified S-W gyrator. One could chose G_4 and G_3 to cancel the positive terms of y_{11} and y_{22} and obtain infinite Q, but this would be an impractically sensitive adjustment; however, enhancement of Q by as much as 10 or 20[5] might reasonably be accomplished without the gyrator becoming unduly sensitive to parameter variations.

Another version of the modified S-W gyrator is shown in Figure 3. This arrangement is useful when Q_1 and Q_2 are reasonably matched along with G_{B1} and G_{B1}, permitting K to be one-half, for then y_{11} and y_{22} may be equally reduced to increase Q by adjustment of G_5 alone.

The S-W gyrator constructed with transistors of the same polarity type can be biased with three current sources as shown in Figure 4. Current sources I_1 and I_2 should, in practical form, be of high impedance whereas current source I_3, because it is connected to a low impedance point in the gyrator circuit, need only to have a high impedance compared to impedance of the emitter circuit of Q_3 and can be in practice a resistor connected to a negative supply voltage. When R_1 and R_2 are equal, the usual case, I_3 must be greater than the sum of I_1 and I_2. The conductances G_3 and G_4 of the modified circuit of Figure 2 or G_5 of Figure 3 are not shown in Figure 4 because these conductances when used are small enough to neglect in bias considerations.

There are several ways of realizing current sources I_1 and I_2. One way is to use transistors, PNP's when the transistors used in the gyrator are NPN's which was the method used in the i.f. amplifier. This results in both PNP and NPN transistors being used in the biased gyrator, usually a disadvantage in integrated circuits, but the current source transistors do not have to be high gain types and lateral type transistors [6] would likely be suitable. Another way is to

use field effect transistors for current sources[4]. Two other methods[4] allowing the transistors of the same polarity type to be used in the gyrator and the biasing circuits are shown in Figure 5. In Figure 5a, Q_4 is used in conjunction with Q_1 which is part of the gyrator circuit to supply current I, due to the substantially constant voltage $(V_Z - V_{BE1} - V_{BE4})$ across resistor R_E. Current source I_2, not shown, may be similarly simulated with the same kind of circuit in association with Q_2 of the gyrator. Figure 5b shows a two-terminal current source that may be used for I_1 and I_2. The two-terminal current source has the voltage-current characteristics shown in Figure 5c. The constant current region extends from a minimum voltage across the circuit of

$$V_{min} \approx 2V_D(1+R_3/R_2) - V_{BE_2} R_3/R_2 + V_{BE_1}, \tag{2}$$

typically about 2.5 volts for equal values of R_2 and R_3 with silicon transistors and diodes, to a maximum voltage marking the break point of the V-I curve where Q_2 cuts off at

$$V_{max} \approx V_{BE_1}(1 + R_3/R_1) + 2V_D(1 + R_3/R_2) - V_{BE_2} R_3/R_2. \tag{3}$$

(In reference [4], where the two-terminal current source is described, contains a serious typographical error).

The gyrator amplifier circuit used in each of the two stages of the i.f. amplifier is shown in Figure 6. Q_4 and Q_5 are PNP transistors used for current sources and Q_6 is an emitter follower to provide a low output impedance. Resistor R_f is for Q enhancement using the method shown in Figure 3.

The input signal is applied to the base of current source Q_4. The voltage transfer function is

$$\frac{V_{out}}{V_{in}} = \frac{R_c(C_2S + g_{22})}{R_1R_{E_1}C_1C_2\left[S^2 + \left(\frac{g_{11}C_2 + g_{22}C_1}{C_1C_2}\right)S + \frac{g_{11}g_{22} - g_{12}g_{21}}{C_1C_2}\right]} \tag{4}$$

where g_{11}, g_{22}, g_{12} and g_{21} are the admittance parameters of the gyrator including the loading effects of the current sources and the effects of Q enhance-

ment. For g_{11}, $g_{22} << g_{12}$, $- g_{21}$, the resonant frequency is

$$\omega_o \approx \sqrt{\frac{-g_{12}g_{21}}{C_1 C_2}} = \sqrt{\frac{1}{R_1 R_2 C_1 C_2}} \qquad (5)$$

and the Q is

$$Q = \frac{\sqrt{-g_{12}g_{21}C_1C_2}}{g_{11}C_2 + g_{22}C_1} . \qquad (6)$$

The voltage gain at resonance is

$$\left| \frac{V_{out}}{V_{in}} \right| (S = j\omega_o) = \frac{Q R_c \sqrt{C_2}}{R_{E_1} R_1 \sqrt{-g_{12}g_{21}C_1}} , \qquad (7)$$

and this reduces to

$$\left| \frac{V_{out}}{V_{in}} \right| (S = j\omega_o) = \frac{Q R_c}{R_{E_1}} , \qquad (8)$$

for $g_{12} = - g_{21} = 1/R_1 = 1/R_2$ and $C_1 = C_2$.

The schematic diagram of the 2-stage 455 kHz i.f. amplifier is shown in Figure 7. The Q of each stage is 29.3 to give a bandwidth of 10 kHz taking into account the bandwidth shrinkage in two single-tuned amplifier stages. The voltage gain for each stage is about 49 and the gain for the two stages is 2400 as predicted by equation (8) and confirmed by measurement.

Different types of transistors were used in each stage to give a Q less than the desired value in one stage and greater than the desired value in the other in order to demonstrate the methods of compensation to bring the Q to the desired value. The Q of the first stage was 16 before being compensated; a feedback resistor of 82 kilohms was used to increase the Q to 29.3. In the second stage the Q of the gyrator was about 50, and port 1 was loaded with a 150 kilohm resistor to reduce the Q to 29.3.

The amplifiers are tuned by a trimmer capacitor at port 1 of each stage. It was necessary to place a decoupling filter in the power supply line to prevent oscillation. Perhaps this could be avoided in an integrated circuit by including a breakdown diode and transistor circuit to regulate the power supply and provide isolation in each amplifier.

B. Gyrator Realization Using Unilateral Amplifiers

A gyrator based on feedback about a unilateral amplifier has been investigated. The concept is as follows: Suppose a conductance g_{fb} is connected between the input and output terminals of a 3-terminal amplifier having

$$\begin{bmatrix} g_{11} & 0 \\ g_m & g_{22} \end{bmatrix} \tag{9}$$

as an admittance matrix. The admittance matrix for the amplifier with the feedback connection is

$$\begin{bmatrix} g_{11} + g_{fb} & -g_{fb} \\ g_m - g_{fb} & g_{22} + g_{fb} \end{bmatrix} \tag{10}$$

It is seen that the y_{12} and y_{21} terms have the opposite signs if g_m is greater than g_{fb}, in which the matrix is that of a stable, lossy, possibly active, gyrator (or positive immittance inverter, PII). The y_{11} and y_{22} terms may be removed or diminished by placing a negative conductances at the two ports[7] by a further modification of the circuit.

How the idea can be worked with transistors is shown in Figure 8. Transistor Q_1 and conductance G_1 make up an amplifier having y_{21} equal to G_1 (assuming ideal transistors) and conductance G_2 is the feedback conductance. Transistor Q_2 together with Q_1 and G_3 form a negative immittance converter to

introduce the $-G_3$ term in the y_{11} element of the gyrator's admittance matrix; similarly, Q_3 and G_4 work with Q_1 to put the $-G_4$ term into the y_{22} element. The matrix in Figure 8 assumes ideal transistors for the purpose of making the operation of the circuit clear. It is seen that the y_{11} and y_{22} elements of the gyrator matrix are made zero when G_3 and G_4 are both equal to G_2. This gyrator is in the class of gyrators Daniels[8] has called active tuned gyrators because the y_{11} and y_{22} terms of the admittance matrix can be tuned to zero leaving an active gyrator or PII. The gyrator is passive when G_1 is zero and G_3 and G_4 are equal to G_2 which makes the y_{12} and y_{21} elements equal in magnitude and of opposite sign.

The collector-base capacitance of Q_1 appears in shunt with G_2 and can introduce losses in an active gyrator of this kind. This capacitive feedback can be reduced by adding another transistor Q_4, as shown in Figure 9, which combines with Q_1 in a cascade circuit. The admittance matrix for this modified circuit is the same as for Figure 8, assuming ideal transistors.

Another modification of the circuit that derives from Figure 9 by relocating one end of G_4 is shown in Figure 10; this may be regarded as a curious interconnection of two negative immittance converters. The admittance matrix for this circuit differs from that of Figures 8 and 9 in that G_4 is removed from the y_{21} element.

The maximum Q of a gyrator with both parts terminated with capacitors is one-half of the square roots of the product of the magnitude of the gyration conductances divided by the square root of the product of the input conductances. For the gyrator of Figures 8 and 9, after letting $G_1 = MG_2$, $G_3 = K_1G_2$ and $G_4 = K_2G_2$, the maximum Q is

$$Q_{max} = 1/2 \sqrt{\frac{M + K_1 + K_2 - 1}{(1 - K_1)(1 - K_2)}} \qquad (11)$$

where K_1 and K_2 must be less than 1 for stability. It is seen that the gyrator is a low Q circuit for the practical reason that in order to obtain high Q, K_1 and K_2 must be nearly unity, i.e. G_3 and G_4 must have values close to G_2 which is difficult adjustment and hard to maintain. The sensitivity of Q_{max} to K_1 is approximately $K_1/1-K_1$, for example, which is high if K_1 is close to one. The sensitivity to M is less than one-half, so M should be as large as possible.

The circuit of Figure 8 was constructed with M 10 and biased with a FET current source connected to the collector of Q_1, a resistor connected to the emitter of Q_2 and returned to a negative supply voltage, and the collector of Q_3 connected to the positive supply voltage. The Q of this gyrator when terminated with capacitors could be made as large as desired by careful adjustment of G_3 and G_4, but it was found that with high Q - of about 50, say - the circuit was sensitive to signal amplitude and biasing. The circuit would function properly with a small signal but would jump to a higher Q condition or break into oscillation when the signal amplitude was increased. This is due, probably, to reduction of the emitter resistances of Q_2 and Q_3, which are part of the conductances G_3 and G_4, during part of the cycle, reducing the input conductances or making them negative.

The circuit is more easily biased than the S-W gyrator, requiring one high impedance current source as compared to two for the S-W gyrator, but in all other respects the S-W gyrator is better.

C. Classification of Gyrators Appearing in Mullaney's Filters

In his thesis work at Northeastern University, R.W. Daniels[8] developed a synthesis procedure for active circuits which he used in a thorough investigation of gyrators of various classes. For each of the classes that he considered, he found all the ways in which the gyrators could be realized with three transistors, this being the minimum number required except for one type of active gyrator. Daniels' classification of gyrators has been useful in understanding the work of others for often active circuits contain gyrators without their presence being noted. In active resonant circuits containing two capacitors as tuning elements, if one regards the circuit as a two-port to which the capacitors are connected; one frequently sees a gyrator between the two ports.

Mullaney[9] has presented a number of active filter circuits having low-pass, band-pass and high-pass characteristics. Two of his low-pass active filter circuits are shown in Figure 11. Some of these circuits contain gyrators in the classes considered by Daniels. For example, Mullaney's Figures 15 and 16 considered as two-ports terminated with capacitors have (with the capacitors removed) an impedance matrix of the following form (assuming ideal transistors):

$$Z = \begin{bmatrix} R_1 - R_2 & -R_2 \\ R_1 & 0 \end{bmatrix} \qquad (12)$$

The impedance matrix represents what Daniels has called a passive tuned gyrator because Z represents a gyrator when R_1 and R_2 are made equal which also makes the gyration resistances equal in magnitude as required for a passive gyrator. Mullaney's Figures 15 and 16 have the same configuration as Daniels' passive tuned gyrator number 2 shown in his Figure 8.9. Mullaney's Figures 23 and 24 are also of this same class and have the same configuration as Daniels' passive tuned gyrator number 10 shown in his Figure 8.17.

Mullaney's Figures 17 through 20 similarly treated have an impedance matrix :

$$Z = \begin{bmatrix} R_2 & -R_2 \\ R_2+R_1 & -R_2 \end{bmatrix} \tag{13}$$

This is in the category of what Daniels calls modified fundamental gyrators, and is a special case of his equation 11.2.17 obtained by letting an additional resistor included by Daniels be zero. Figures 21 and 22 of Mullaney also contain gyrators of this type.

D. Geffe's Q-Invariant Resonator and the S-W Gyrator Compared

Geffe[10] has shown that the pole Q of the active resonator of Figure 12 has zero differential sensitivities to the passive elements, as does the circuit formed by interchanging the R's and C's in the circuit.

It is interesting to compare Geffe's circuit which uses voltage amplifiers with the S-W gyrator of Figure 1 which uses current amplifiers.

Geffe's circuit contains a gyrator (or PIT) which is found by removing the two capacitors and calling the places to which they were connected the ports of the gyrator. The gyrator in Figure 12 has

$$Z = \begin{bmatrix} R_1 & -A_1R_1 \\ -A_2R_2 & R_2 \end{bmatrix} \tag{14}$$

for its impedance matrix (one amplifier being an inverting and the other being a noninverting type in order to have a gyrator or a resonator).

Treating the other version of the circuit (formed by interchanging R's and C's) in the same way uncovers another gyrator having the following admittance matrix:

$$Y = \begin{bmatrix} 1/R_1 & -A_2/R_1 \\ -A_1/R_2 & 1/R_2 \end{bmatrix} \tag{15}$$

where one of the amplifiers is an inverting type and the other is a noninverting type.

The S-W gyrator of Figure 1 has an admittance matrix (assuming ideal transistors or ideal current amplifiers) as follows:

$$Y = \begin{bmatrix} 1/A_1R_1 & 1/R_2 \\ -1/R_1 & 1/A_2R_2 \end{bmatrix} \tag{16}$$

where $A_1 = \beta_1 + 1$ and $A_2 = \beta_2 + 1$. If the ports and resistors are interchanged, another gyrator (reference 5, Figure 4.5b) having an impedance matrix

$$Z = \begin{bmatrix} R_1/A_1 & -R_2 \\ R_1 & R_2/A_2 \end{bmatrix} \tag{17}$$

is obtained.

From examination of the matrices of the two circuits, it is seen that in Geffe's circuit the gyration conductances or impedances are the input conductances or impedances multiplied by the amplifier voltage gains, whereas in the S-W

circuit the input and output conductances or impedances are the gyration conductances or impedances divided by the amplifier current gains. For both circuits the maximum resonator Q is the same:

$$Q_{max} \approx (A_1 A_2)^{1/2}/2. \tag{18}$$

for Geffe's circuit:

$$\omega_o = \frac{1}{\sqrt{(1-A)T_1 T_2}} \tag{19}$$

and

$$Q = \frac{\sqrt{(1-A)T_1 T_2}}{T_1 + T_2} \tag{20}$$

where $A = A_1 A_2$, $T_1 = R_1 C_1$, and $T_2 = R_2 C_2$.
The sensitivities are:

$$S_{T_1}^{\omega_o} = S_{T_2}^{\omega_o} = -1/2 \tag{21}$$

$$S_A^{\omega_o} = A/2(1-A) \tag{22}$$

$$S_A^{Q} = -A/2(1-A) < 1/2 \tag{23}$$

$$S_{T_1}^{Q} = 1/2 - T_1/(T_1 + T_2) = 0, \text{ if } T_1 = T_2. \tag{24}$$

$$S_{T_2}^{Q} = 1/2 - T_2/(T_1 + T_2) = 0, \text{ if } T_1 = T_2. \tag{25}$$

For the S-W circuit:

$$\omega_o = \frac{1}{\sqrt{T_1 T_2 (1 + 1/A)}} \tag{26}$$

$$Q = \frac{\sqrt{T_1 T_2 A (1 + A)}}{T_1 A_2 + T_2 A_1} \tag{27}$$

The sensitivities are:

$$S_{T_1}^{\omega_o} = S_{T_2}^{\omega_o} = -1/2 \tag{28}$$

$$S_A^{\omega_o} = 1/2(1 + A) \tag{29}$$

$$S_{T_1}^{Q} = 1/2 - T_1A_2/(T_1A_2 + T_2A_1) = 0, \text{ if } T_1A_2 = T_2A_1. \tag{30}$$

$$S_{T_2}^{Q} = 1/2 - T_2A_1/(T_1A_2 + T_2A_1) = 0, \text{ if } T_1A_2 = T_2A_1. \tag{31}$$

$$S_{A_1}^{Q} = \frac{(1 + 2A)}{2(1 + A)} - \frac{T_2A_1}{T_1A_2 + T_2A_1} < 1/2, \text{ if } T_1A_2 = T_2A_1. \tag{32}$$

$$S_{A_2}^{Q} = \frac{(1 + 2A)}{2(1 + A)} - \frac{T_1A_2}{T_1A_2 + T_2A_1} < 1/2, \text{ if } T_1A_2 = T_2A_1. \tag{33}$$

The sensitivities of both Geffe's resonator and the S-W gyrator are low. Both can be made to have the Q insensitive to the passive elements, but this is more easily done with Geffe's circuit because it only requires matching time constants while the S-W circuit requires matching products of time constants and amplifier gains. The S-W circuit's resonant frequency is less sensitive to amplifier gains than Geffe's circuit, and Geffe's circuit has better Q stability.

E. Gyrator Realization Using Cascaded NIC's.

1.0 Introduction: The ideal gyrator is part of a class of active element building blocks called a Positive Immittance Inverter (PII). The other building blocks are the Negative Immittance Inverter (NII), the Positive Immittance Converter (PIC) and the Negative Immittance Converter (NIC). Each of these blocks may be considered as two-port networks whose characteristics are defined by the impedance seen at one port in relation to the terminating impedance at the second port. Figure 13 is useful in demonstrating these properties. All four basic circuits are governed by the relation,

$$Z_{in} = \pm kW_L \tag{34}$$

where k is the conversion ratio and W_L is the load immittance (impedance or admittance). If $W_L = Z_L$, Equation (34) defines the PIC and NIC, while if $W_L = Y_L$, the PII and NII result.

The four building blocks are not independent and form a redundant set. Any three can be used to synthesize the remaining one. Generally, only two basic circuits are required, one inversion type and one conversion type, provided one of the two blocks reflects a negative impedance. The concept of interconnecting basic building blocks is the basis for the gyrator realization presented herein. Included in the report are the theoretical bases for the realization, the actual circuit realizations, including biasing considerations, and the experimental results obtained.

1.1 Theoretical Basis: The gyrator as a circuit element, is defined by Equation (35).

$$\left[Z_{gyr}\right] = \begin{bmatrix} 0 & \alpha \\ \alpha & 0 \end{bmatrix} \tag{35}$$

where α is called the gyration resistance. The PII characteristic may be obtained by cascading NIC and NII circuits.[11, 12] As shown in Figure 14, the NII inverts the impedance and the NIC provides the additional negative sign to give a positive conversion ratio. Based on the transmission(ABCD)matrices for the NII and NIC, $[Z_{gyr}]$ becomes

$$\left[Z_{gyr}\right] = \begin{bmatrix} 0 & R \\ -R & 0 \end{bmatrix} \tag{36}$$

where

Circuits for the realization of NIC's are well known[13, -17]those for NII circuits less so. The most elementary NII's are shown in Figure 15. As described in reference [11], tunnel diodes are used to provide the negative resistance required. Biasing, small dynamic range, and potential stability problems limit the use of tunnel diodes. Additionally, the incompatability of fabricating single-chip integrated circuits using both tunnel diodes and transistors is a serious drawback.

The proposed realization for the NII utilizes the NIC as a basic building block as shown in Figure 16. The terminating resistance on the NIC provides the negative resistance in the shunt branch (see Figure 15). The resulting structure uses two NIC circuits to realize the basic gyrator and is depicted in Figure 17.

1.2 The Circuit Realizations: The basic NIC circuit, shown in Figure 18, is based on that proposed by Nagata[18]. The advantages of using this circuit is that it requires no circuit adjustment or interval bias supplies. The circuit characterization is controlled primarily by the external resistors. For transistors whose β_o is large, the negative resistance, R_N is given as

$$R_N \approx -\frac{R}{r} R_L \tag{37}$$

so that the conversion ratio $k = R_L/r$.

Figure 19 depicts the i-v characteristic of the input port of the resistively loaded NIC. It is evident that the negative resistance region is quite linear and may be thought of as a "current controlled" negative resistance allowing for current source biasing. This biasing is convenient in transistor circuits.

The NII is generated from the NIC by adding two series resistors (to complete the Tee) each of value of $+R_N$. This circuit, with the appropriate biasing scheme is shown in Figure 20. The resistors R_1 and R_2 are adjusted so that z_{11} and z_{22} of the NII are approximately zero.

To complete the gyrator, a second NIC is required. It is necessary that the load on this NIC be equal to the d-c resistance seen looking into the NII input so that direct coupling may be employed. Elimination of the coupling capacitor reduces interstage loading problems and alleviates the stability problem associated with negative impedance devices.

The complete gyrator realization is shown in Figure 21. One constant current source is required to bias the entire circuit. The NIC and NII portions are easily identifyable. The direct coupling and reasonable resistor ranges appear to permit integrated circuit realization. The major difficulty will be to realize the PNP and NPN transistors simultaneously.

1.3. Circuit Performance: Measurements to determine the z-parameters of the gyrator. The initial measurements obtained resulted in

$$\begin{aligned} z_{11} &= -1.15 \times 10^{-5}\,s & z_{12} &= -1050\,\Omega \\ z_{21} &= 207\,\Omega & z_{22} &= 0.44 + 6.35 \times 10^{-5}\,s \end{aligned} \tag{38}$$

The slight inductive terms in z_{11} and z_{22} may be significantly reduced by the inclusion of a small capacitance across port two of the gyrator. This is the 56 pf capacitor shown in Figure 21. This capacitor reflects into the input of the gyrator as k^2/z_L; that is, as a positive inductance which tends to cancel

z_{11}.

Based on the addition of the 56 pf capacitor, and slight adjustment in the biasing scheme a new set of z-parameters were determined. These resulted in

$$z_{11} = 0.35 \times 10^{-6} s \qquad z_{12} = -1050\,\Omega$$

$$z_{21} = 207\,\Omega \qquad z_{22} = 6.4 \times 10^{-5} s + \frac{1.8 \times 10^{10}}{s} \qquad (39)$$

The values given by (39) correspond to an asymptotic Bode diagram fit for the frequency range 100 Hz to 1MHz. While unable to obtain specific measured values (because of their extremely small size), the resistive portions of z_{11} and z_{22} were determined to be less than 0.01 ohm. These asymptolic plots are shown in Figure 22 a, b, c, d.

Equations (38) and (39) both indicate that the gyrator realization of Figure 21 is an active, non-reciprocal PII. Most gyrator realizations reported thus far are reciprocal and thus passive PII's. If one were to reverse the cascade; . ., NII-NIC,, the magnitudes of z_{12} and z_{21} would probably be reversed. This was not attempted because of the potential stability problems. The activity may be measured by considering the z-matrix of the gyrator as the series combination of two two-port networks. One possible decomposition is given by

$$\begin{bmatrix} z_{gyr} \end{bmatrix} = \begin{bmatrix} 0.35 \times 10^{-6} s & -1050 \\ +1050 & 6.4 \times 10^{-5} s + \frac{1.8 \times 10^{10}}{s} \end{bmatrix} + \begin{bmatrix} 0 & 0 \\ -780 & 0 \end{bmatrix} \qquad (40)$$

The first matrix represents the reciprocal gyrator while the second is interpreted as a current-controlled voltage source. The potential gain from this circuit is attributed to the nonreciprocal nature.

The use of this gyrator at low frequencies (audio) to simulate tuned circuits was also determined. By terminating port two by a capacitor C_L, an induction L is presented at port one. For C_L=0.123uF an inductance of L = 26 mH is attained at port 1. At a frequency of 10 kHz, this inductor should theoretically have a Q of 16×10^4. Because of the limitation in measuring equipment, and the inherent Q of the capacitors available, the Q of the simulated coil was determined to be greater than 5000.

The gyrator was also loaded as a series resonant circuit at 10kHz as depicted in Figure 23. As expected, a sharp notch was obtained; the experimental data shown in Figure 24. From the curve of Figure 24, the Q of the circuit is obtained as 1200 + 100 for several different Δf values. The Q of this circuit is limited more by the signal source used in measurement than the loading of the gyrator.

1.4 Summary: The NIC-NII cascade technique for realization of a gyrator appears successful at low frequencies. The NII circuit derived from an NIC is convenient in design, particularly in integrated circuits. The final circuit developed is a convenient direct-coupled circuit which requires a single source and has a common ground throughout. The quality factors obtained for both the gyrator and gyrator notch circuit compare favorably with those reported in the literature to date.

The device has two limitations. The first is that port one is open-circuit stable and therefore should be driven from a current source. The second is that the performance is very sensitive to the resistors R_1 and R_2. This, too, is typical of negative impedance circuits where positive and negative ports must cancel.

In summary, the NIC-NII cascade realization of PII circuits is feasible and is comparable in performance to other developed techniques.

References

1. Sipress, J.M. and F.S. Witt, U.S. Patent No. 3,001,157; 19 Sept. 1961.

2. Rao, T.N., Gary, P. and R.W. Newcomb, "Equivalent Inductance and Q of a Capacitor-Loaded Gyrator," IEEE Journal of Solid State Circuits (Correspondence) Vol. SC-2, No. 1, pp. 32-33, March 1967.

3. Bach, R.E., Jr., A.W. Carlson, G.F. Currin and P.R. Scott, "Reliable Solid-State Circuits," Semiannual Report No. 5, NASA NGR-22-011-007, Northeastern University, Boston, Mass. 1 July 1967.

4. Cochrun, B.L., A.W. Carlson, W.B. Nowak, "Inter-Relations Between Advanced Processing Techniques Integrated Circuits, Materials Development and Analysis," Scientific Report No. 1, NASA NGR-22-011-007, Northeastern University, Boston, Mass. 1 January 1969.

5. Gensel, J. "Notes on the Structure of Gyrator Circuits," Proc. IEEE (Letters), Vol. 55, No. 10, Oct. 1967, pp. 1735-1736.

6. Lin, H.C., T.B. Tan, G.Y. Chang, B. Van Der Leest and N. Formivgoni, "Lateral Complementary Transistor Structure for the Simultaneous Fabrication of Functional Blocks," Proc. IEEE, Vol. 52, No. 12, Dec. 1964.

7. Bogert, B. P., "Some Gyrator and Impedance Inverter Circuits," Proc. of IRE, Vol. 43, No. 7, July 1955, pp. 793-796.

8. Daniels, R.W., "A Synthesis Procedure for Gyrators and Related Circuits," Ph.D. Thesis, Northeastern University, Boston, Mass., Feb. 1969.

9. Mullaney, Jack W., "Active Filters: Part 11, Varying the Approach," Electronics, Vol. 42, No. 15, July 21, 1969, pp. 86-93.

10. Geffe, Phillip R., "A Q-Invariant Active Resonator," Proc. IEEE (Letters), Vol. 57, No. 8, August 1969, pp. 1442.

11. Grabel, A., "The Use of Sensitivity as a Criterion in the Synthesis of Active Networks," Doctoral Dissertation, New York University, 1964.

12. Ghausi, M.S., "Principles and Design of Linear Active Circuits," McGraw-Hill, 1965.

13. Linvill, J.G., "Transistor Negative Impedance Converters," Proc. IRE, Vol. 41, pp. 725-729, June 1953.

14. Sandberg, I.W., "Synthesis of Driving Point Impedances with Active RC Networks," BSTJ, Vol. 39, pp. 947-962, July 1960.

15. Larky, A.I., "Negative Impedance Converters," IRE Transactions, Vol. CT-4, pp. 124-131, September 1957.

16. Myers, R. B., "Transistor RC Network Synthesis," IRE Wescon Convention Record, Part 2, 1959.

17. Lundry, W. R. "Negative Impedance Circuits: Some Basic Relations and Limitations," IRE Transactions, Vol. CT-4, pp. 132-139, September 1957.

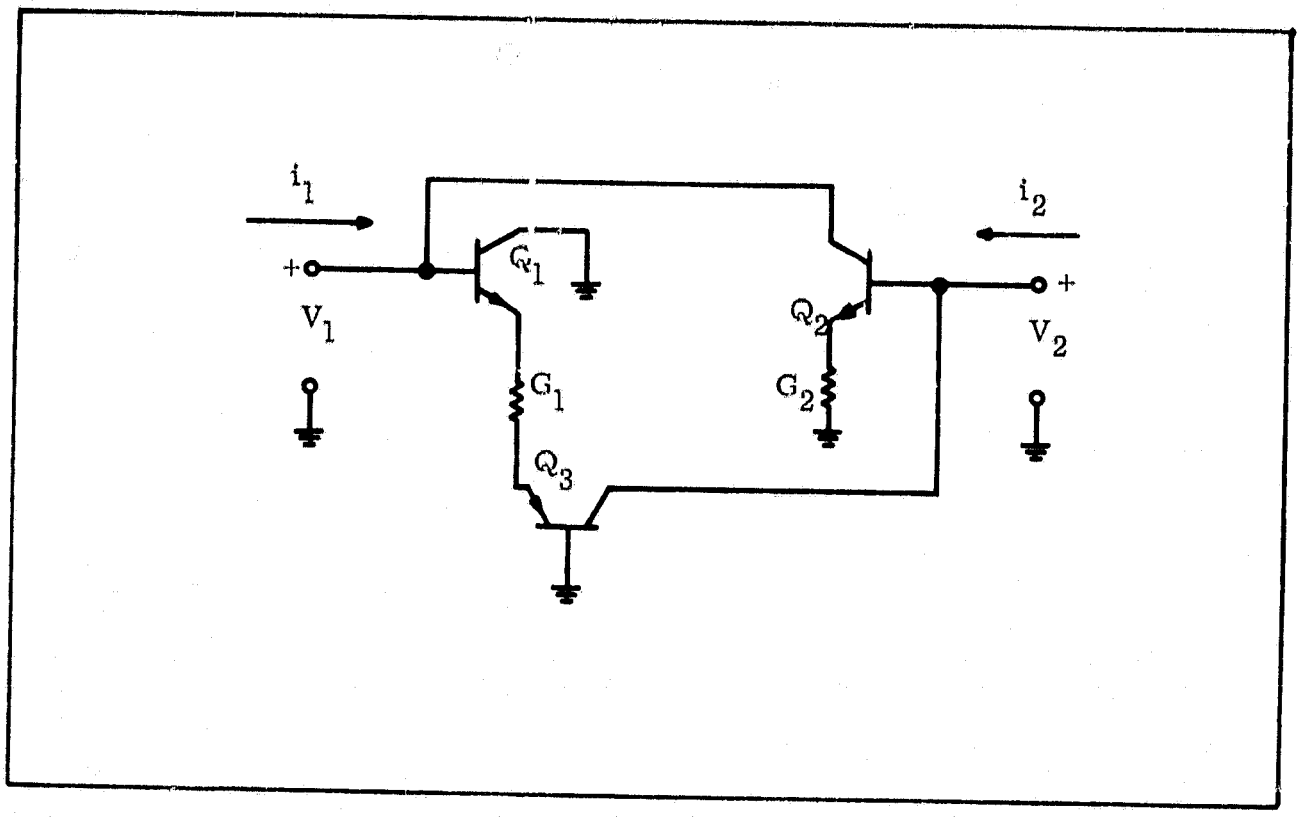

$$y \approx \begin{bmatrix} (1-\alpha_1)G_1 & \alpha_2 G_2 \\ -\alpha_3 G_1 & (1-\alpha_2)G_2 \end{bmatrix}$$

Figure 1. Basic Circuit of S-W Gyrator

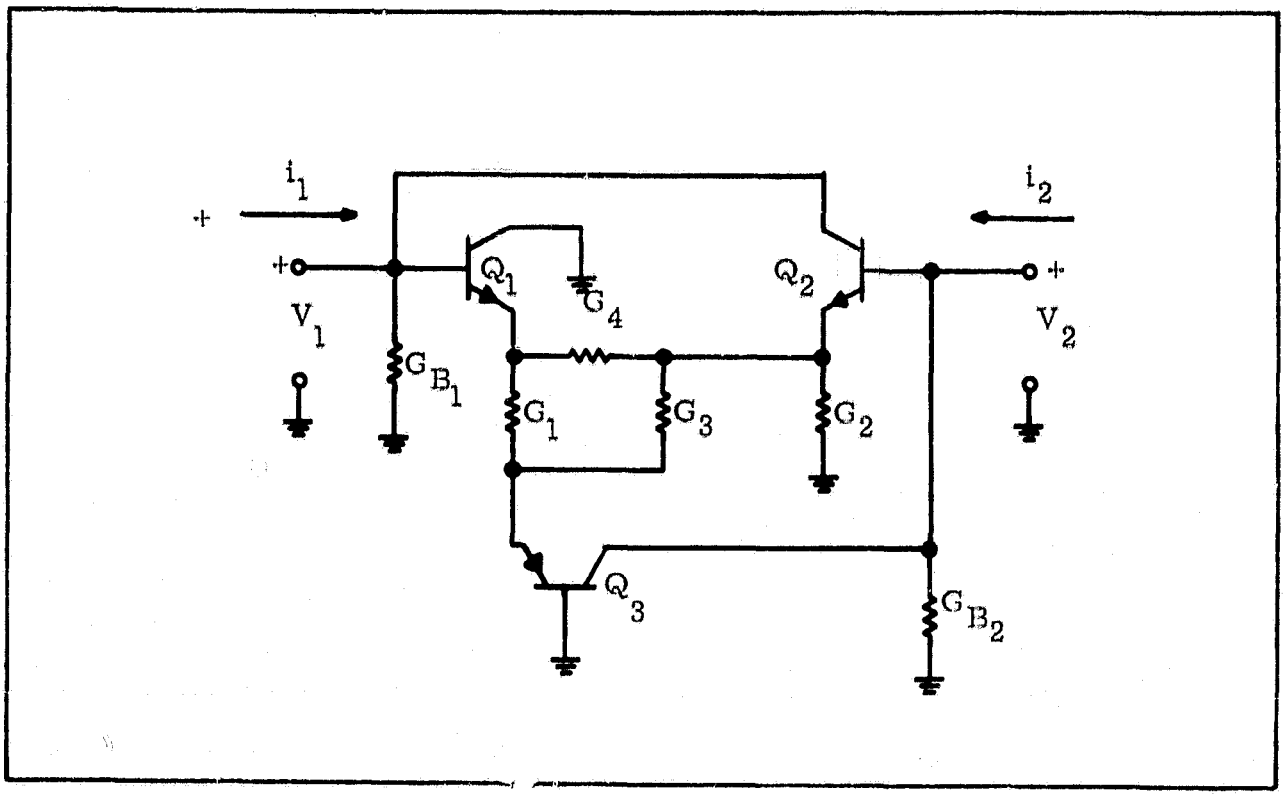

$$y \approx \begin{bmatrix} [(1-\alpha_1)(G_1+G_4)+G_{B1}-G_4] & \alpha_2(G_2+G_3+G_4) \\ -\alpha_3 G_1 & [(1-\alpha_2)(G_2+G_3+G_4)+G_{B2}-G_3] \end{bmatrix}$$

Figure 2. Modified S-W Gyrator

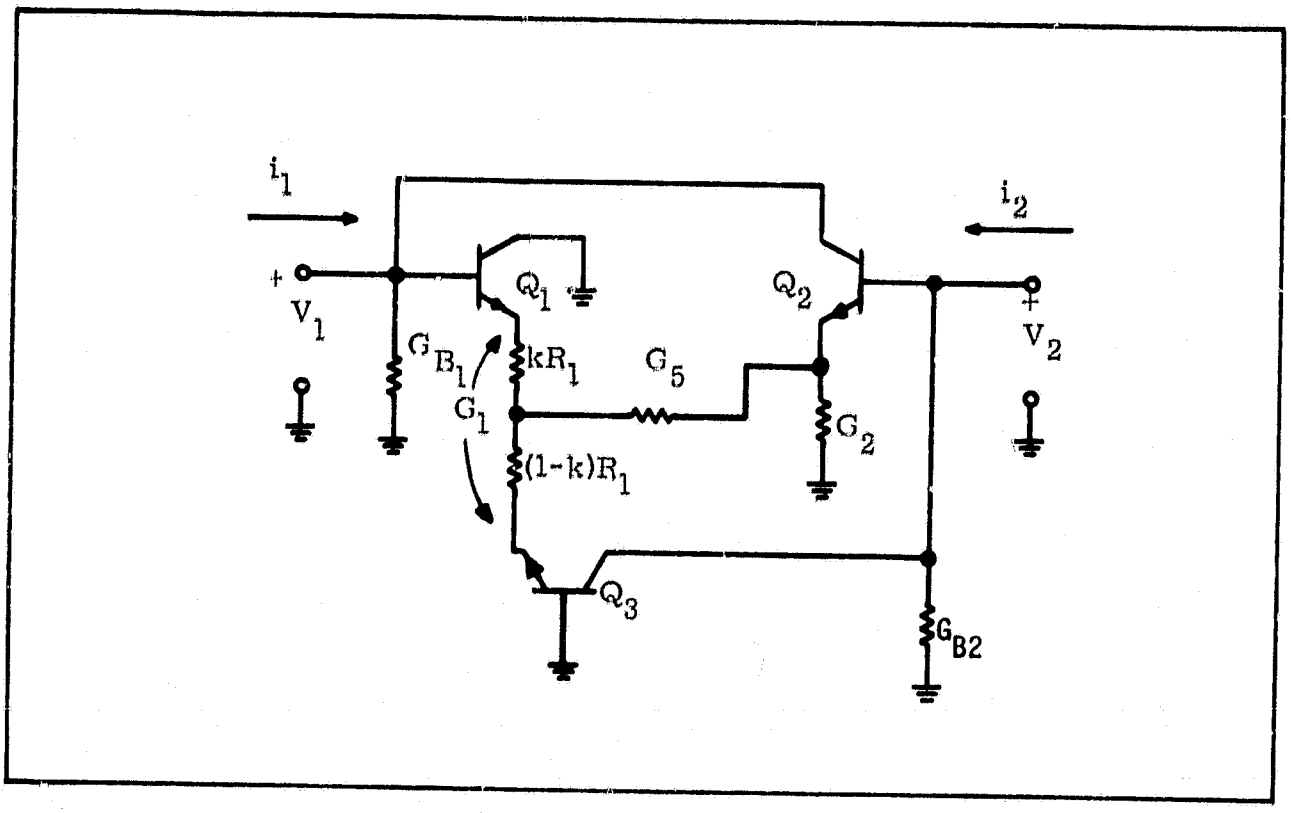

for $G_5 << G_1$ $\qquad 0 < k < 1$

$$y \approx \begin{bmatrix} [(1-\alpha_1)G_1 + G_{B1} - (1-k)\alpha_2 G_5] & \alpha_2(G_2+G_5) \\ -\alpha_3 G_1 & [(1-\alpha_2)(G_2+G_5) + G_{B2} - k\alpha_3 G_5] \end{bmatrix}$$

Figure 3. Another Version of Modified S-W Gyrator

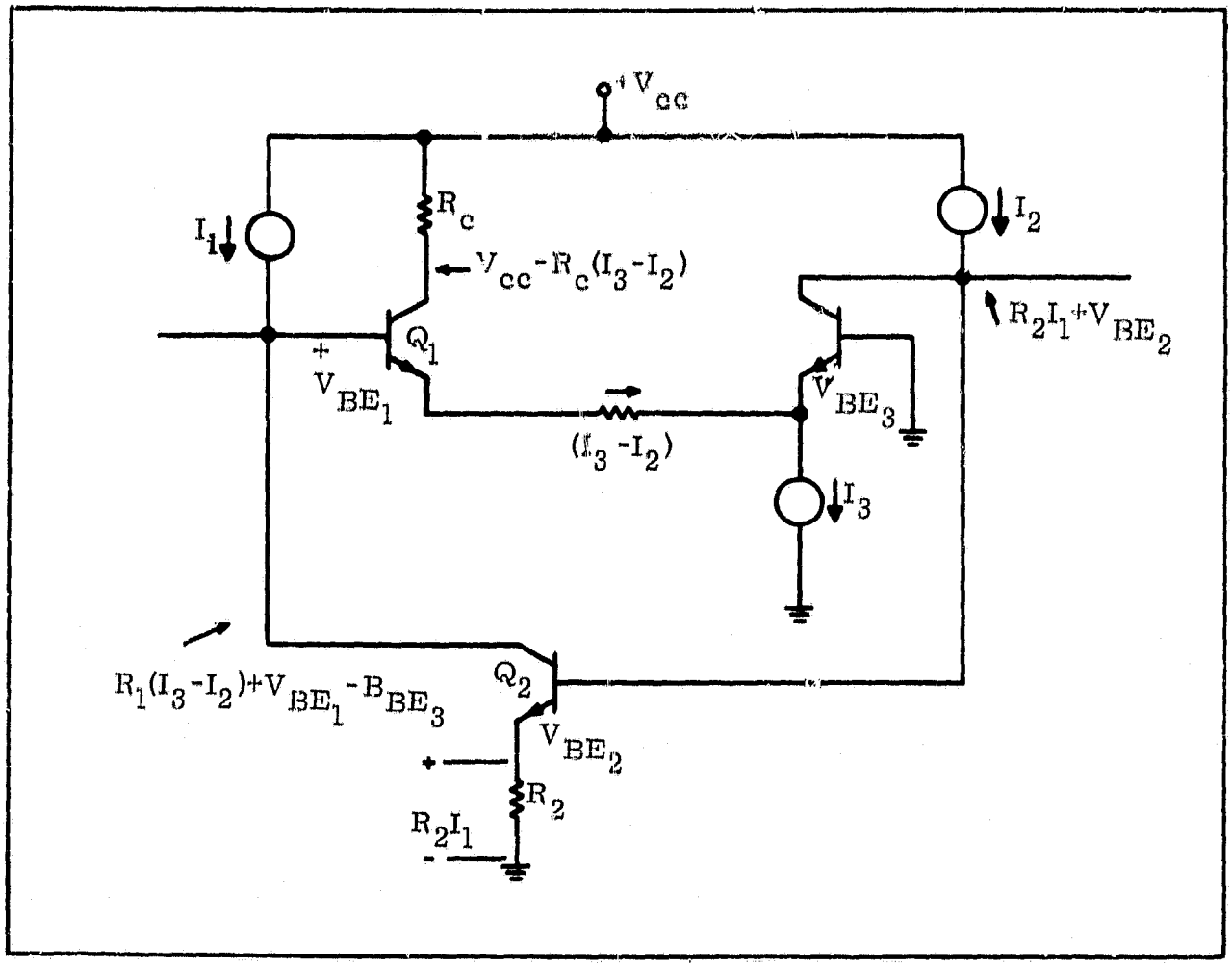

For Q_2 to be active: $R_1(I_3 - I_2) > R_2 I_1$ (assuming $V_{BE_1} = V_{BE_3}$)

For Q_1 to be active: $V_{cc} + V_{BE_3} > (R_1 + R_c)(I_3 - I_2)$

Figure 4. Biasing S-W Gyrator

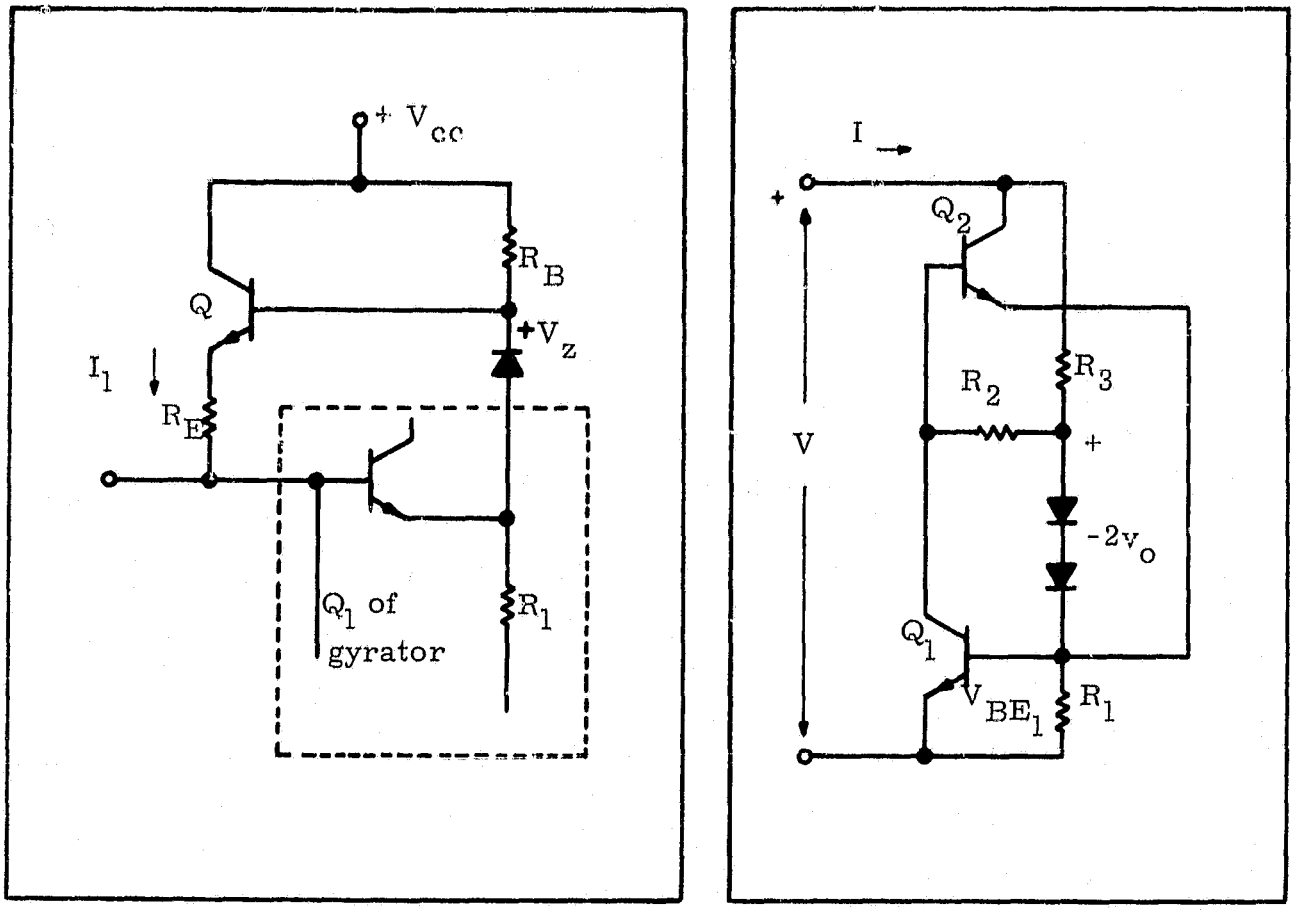

a) Transistor Current Source

b) Two-Terminal Current Source

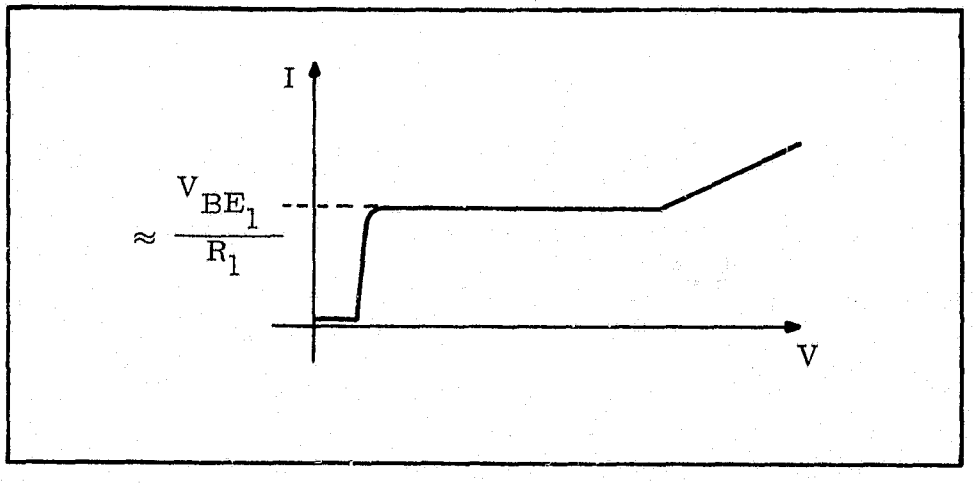

c) V-I Characteristic of Two-Terminal Current Source

Figure 5. Other Means of Current Source Biasing S-W Gyrator

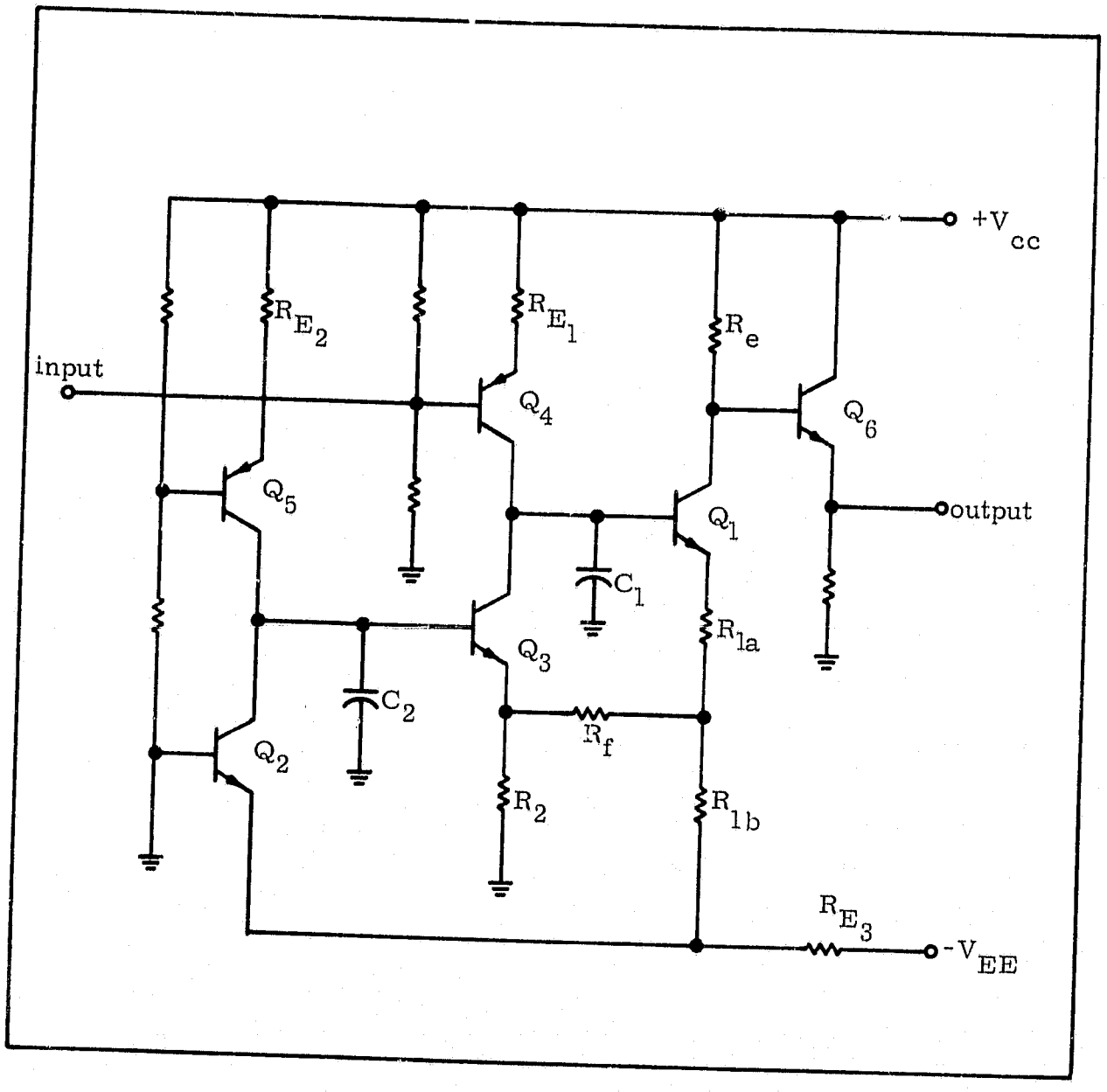

Figure 6. Gyrator-Amplifier Circuit

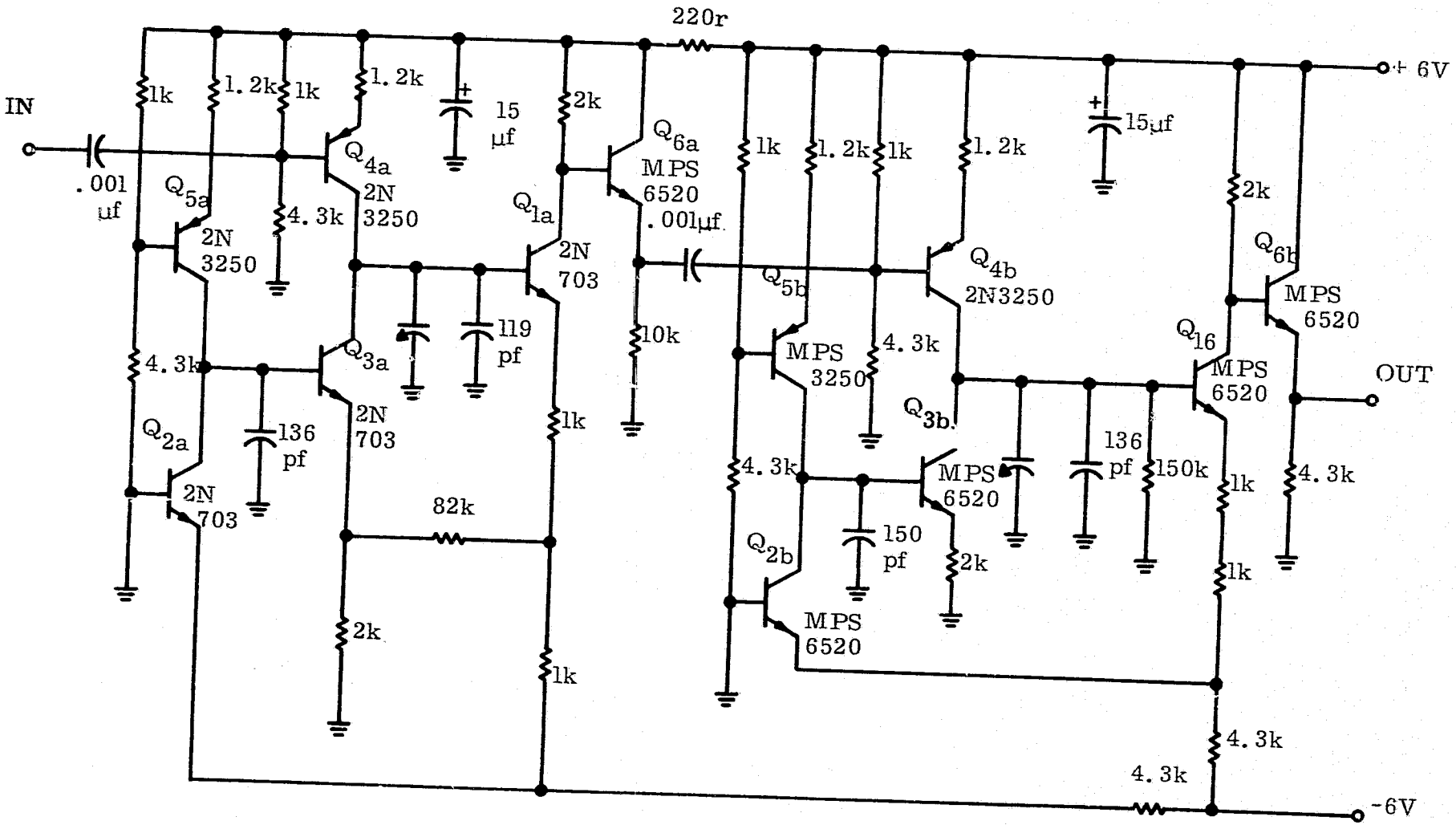

Figure 7. 455 kHz IF Amplifier

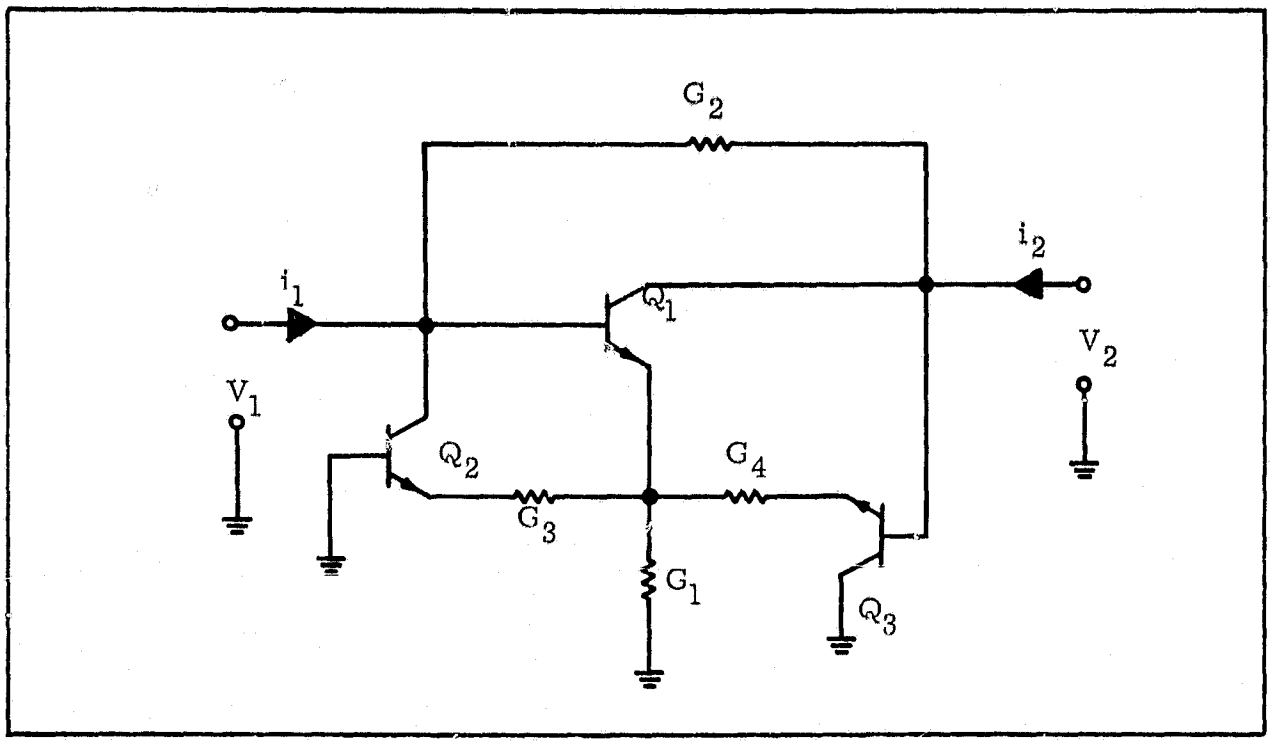

$$Y = \begin{bmatrix} G_2 - G_3 & -G_2 \\ G_1 + G_3 + G_4 - G_2 & G_2 - G_4 \end{bmatrix}$$

Figure 8. A Gyrator Circuit

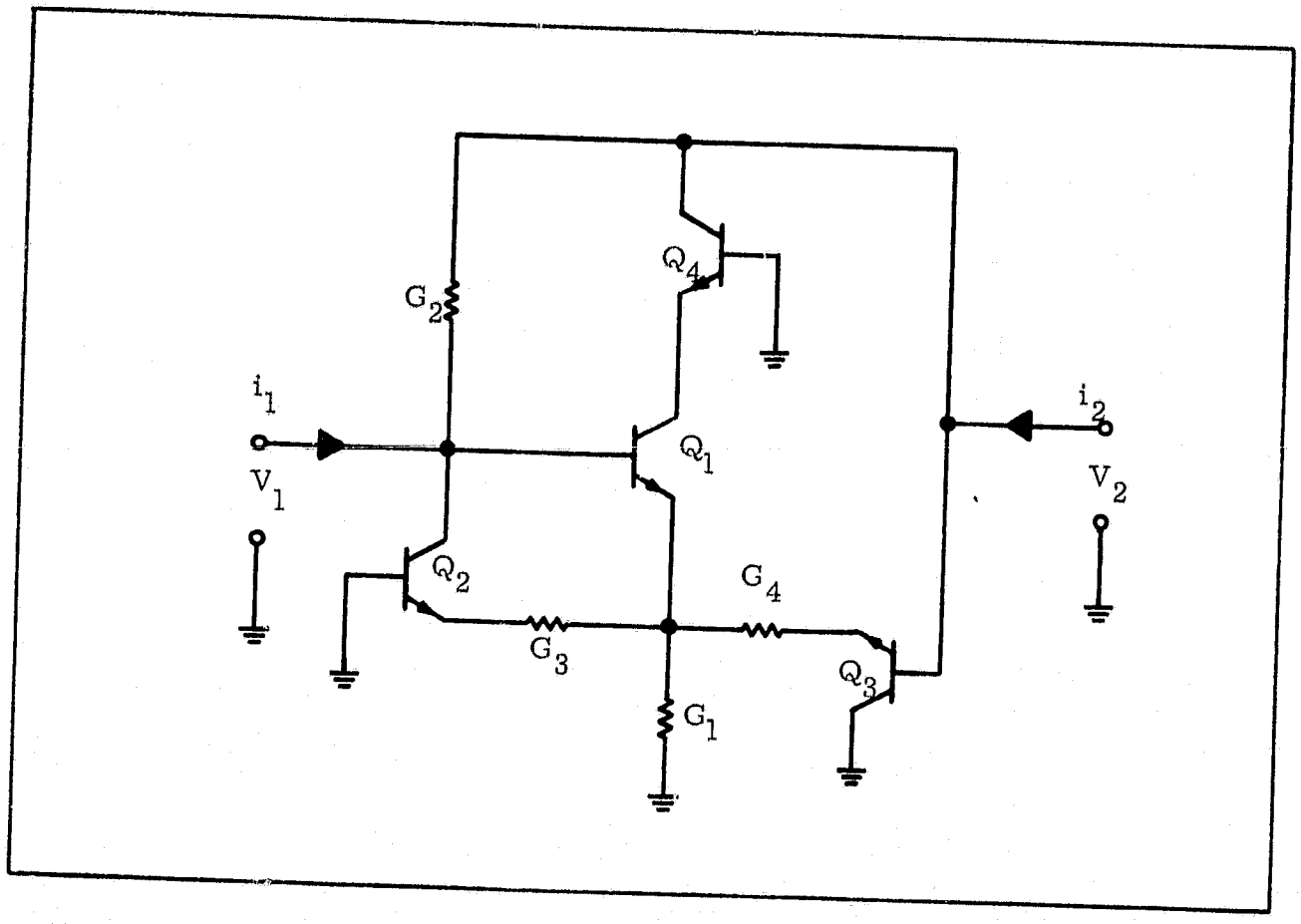

Figure 9. A Modification of Figure 7

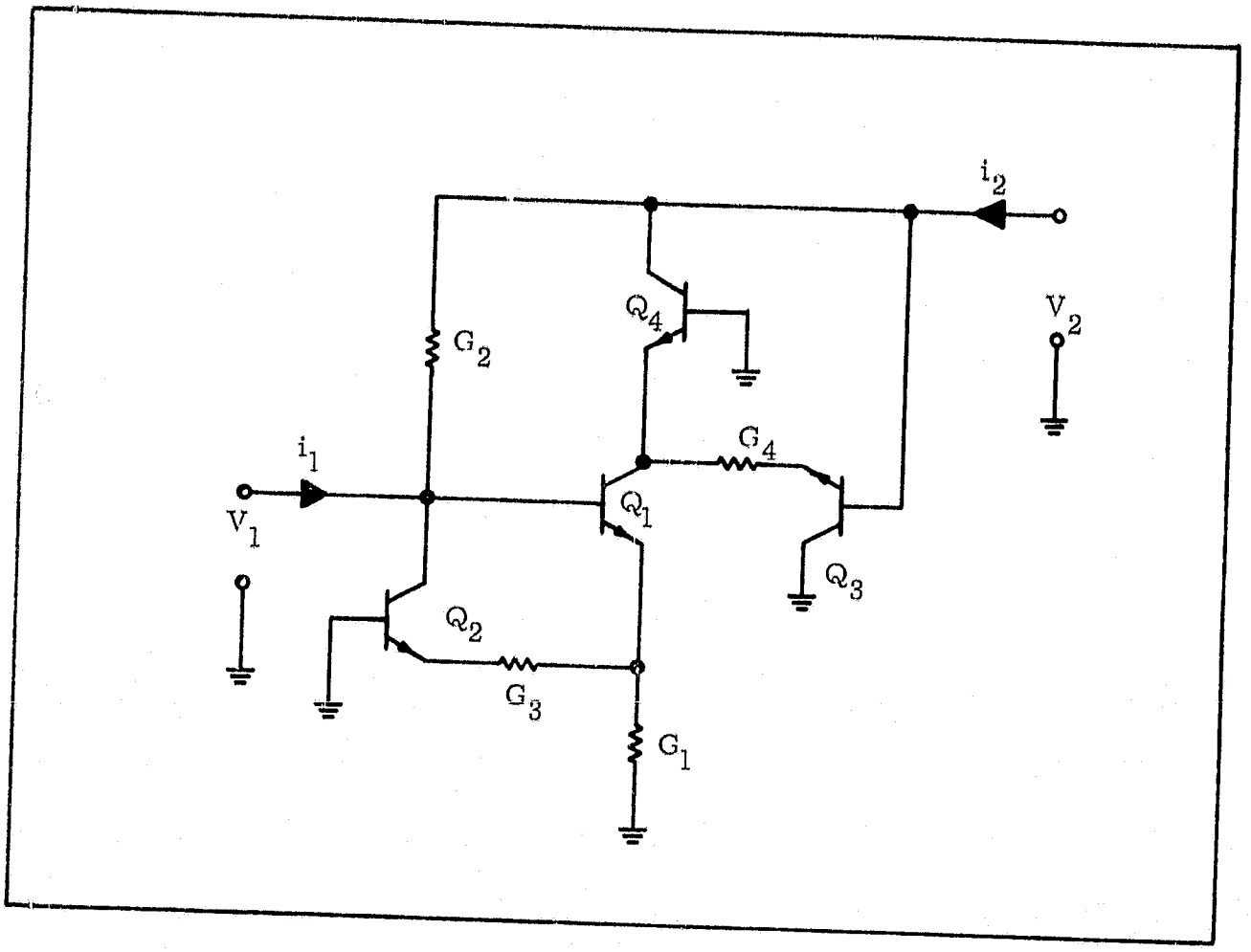

$$y = \begin{bmatrix} G_2 - G_3 & -G_2 \\ G_1 + G_3 - G_2 & G_2 - G_4 \end{bmatrix}$$

Figure 10. Another Modification of Figure 7

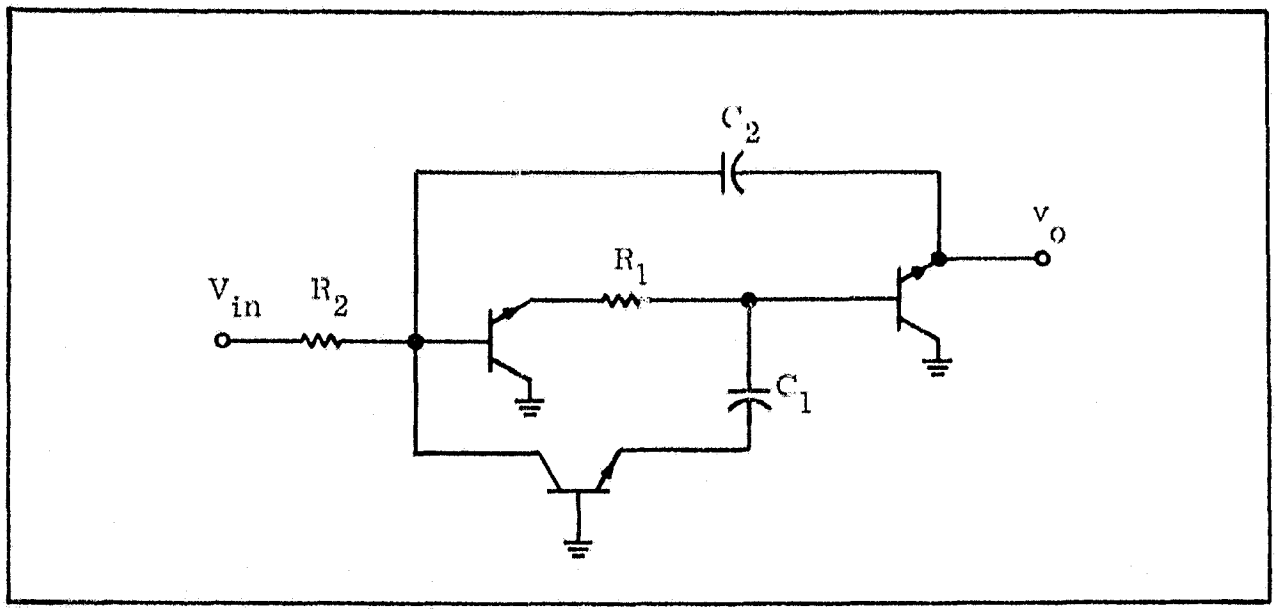

a) Mullaney's Figure 15

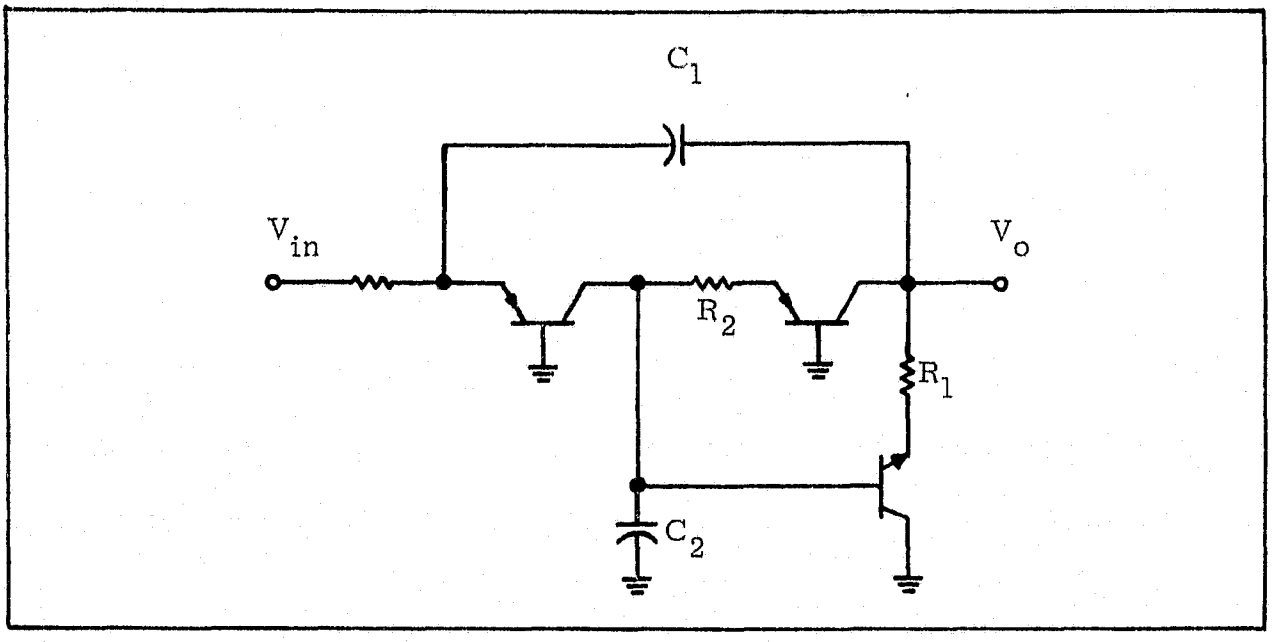

b) Mullaney's Figure 17

Figure 11. Some of Mullaney's Active Filter Circuits

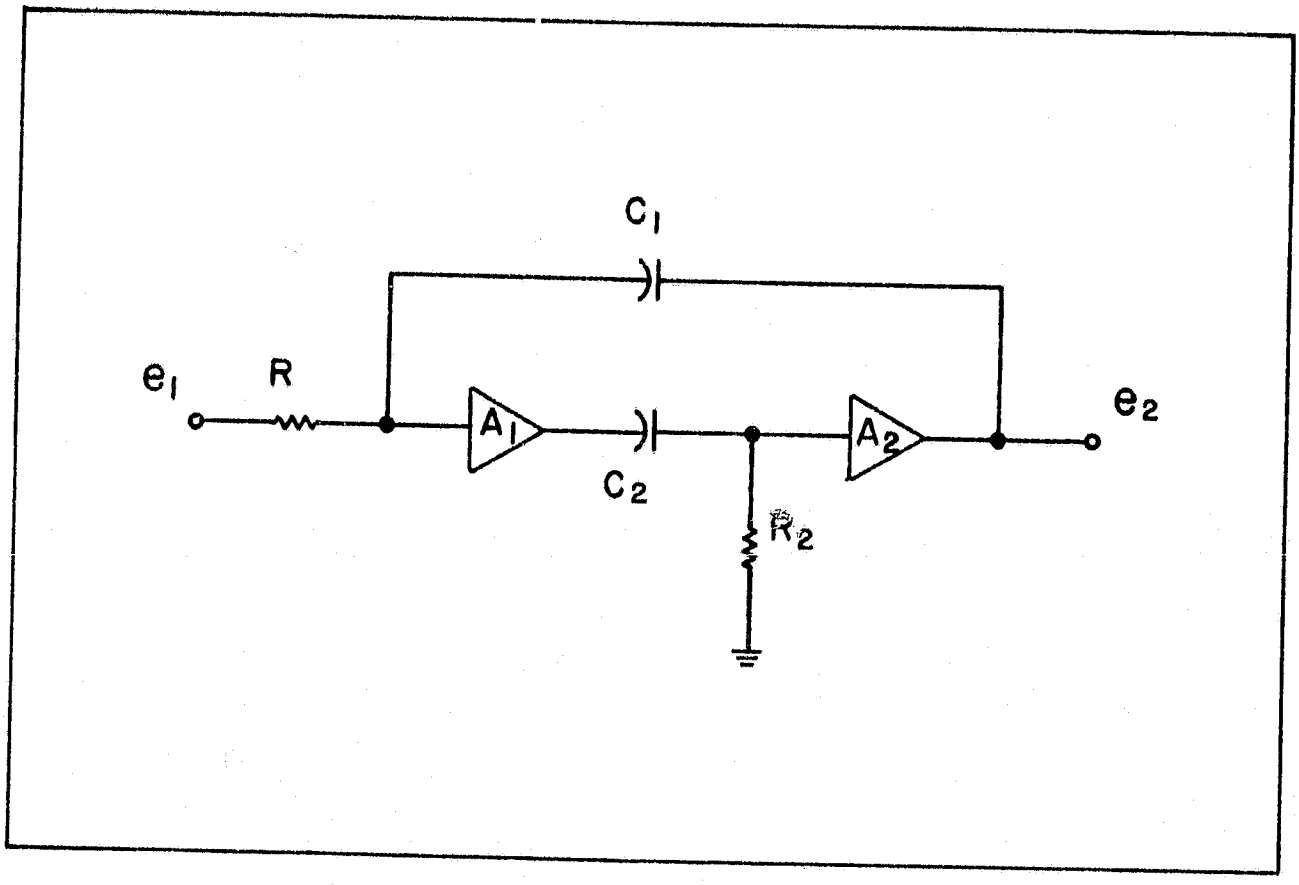

Figure 12. Geffe's Q-Invariant Resonator

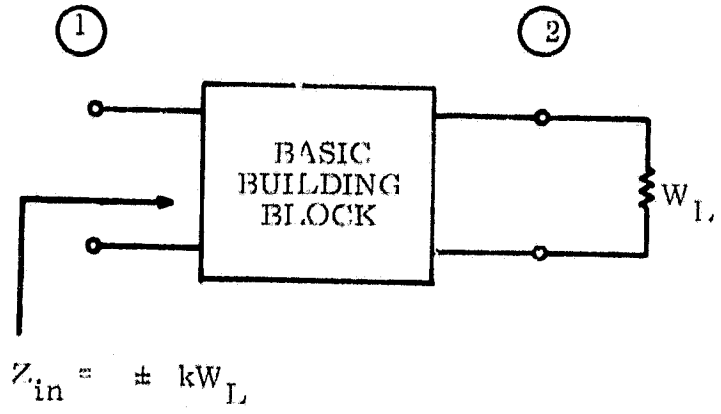

Figure 13. Defining Relationship for Basic Building Blocks

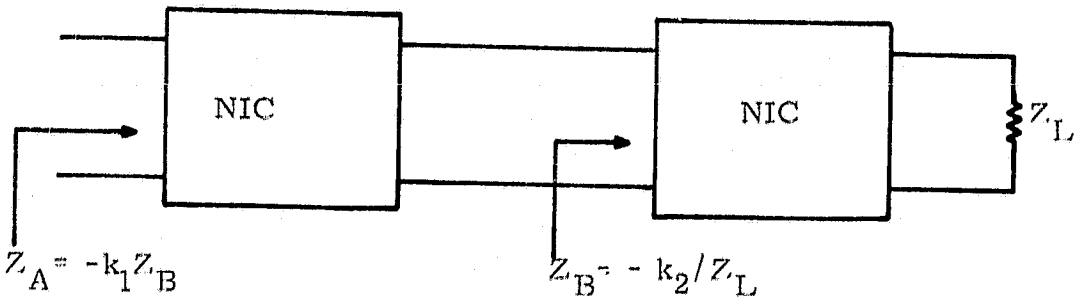

Figure 14. The NIC-NII Cascade Realization of the Gyrator

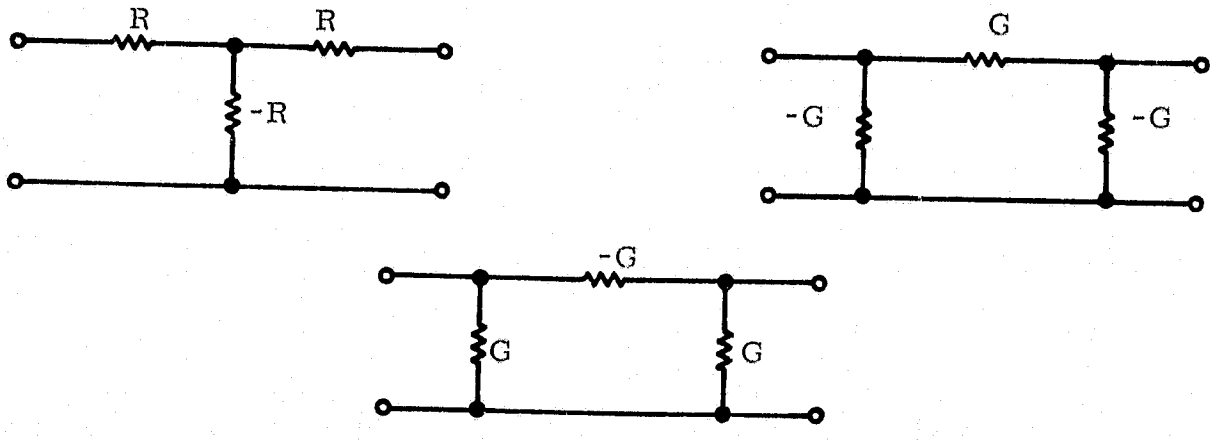

Figure 15. Elementary Realizations of NII Circuits

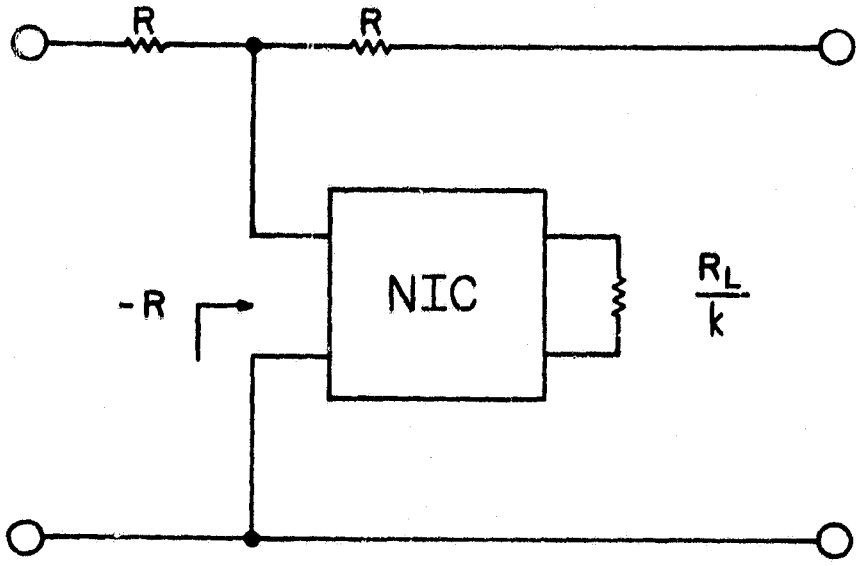

Figure 16. An NII Realization Based on an NIC Circuit

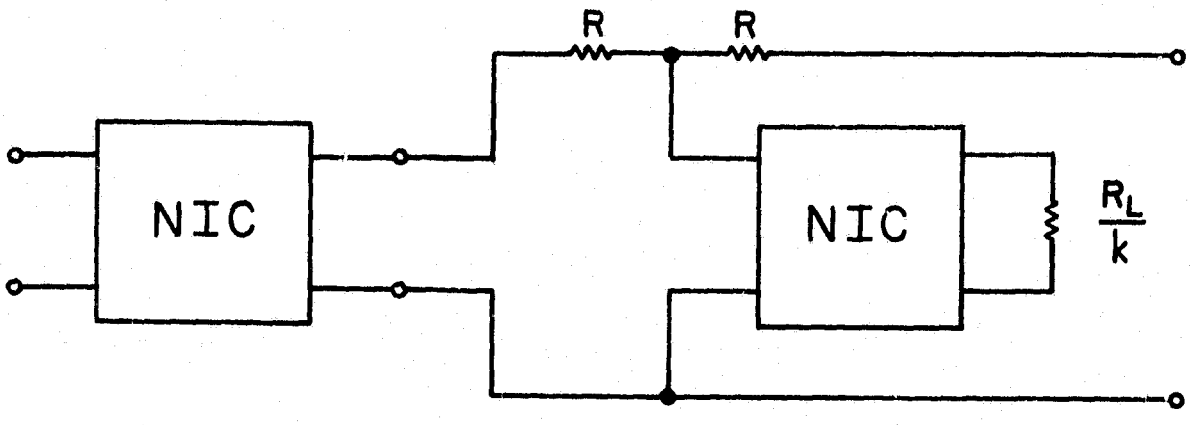

Figure 17. A Two NIC Gyrator Realization

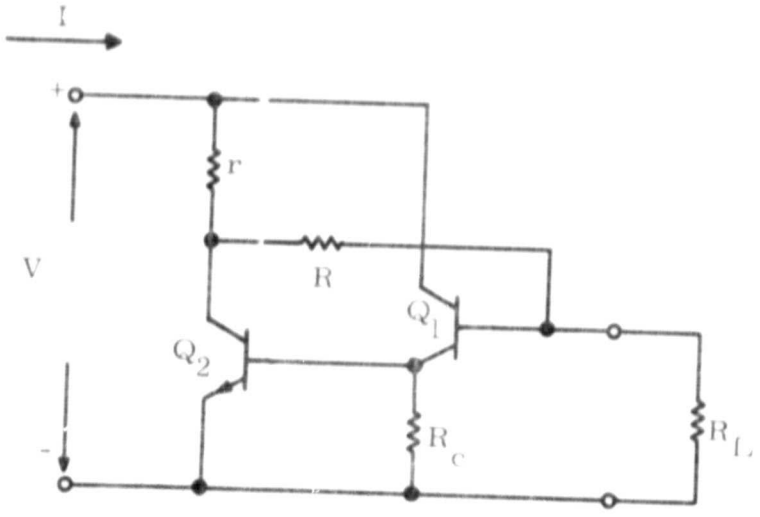

Figure 18. The Basic NIC Circuit

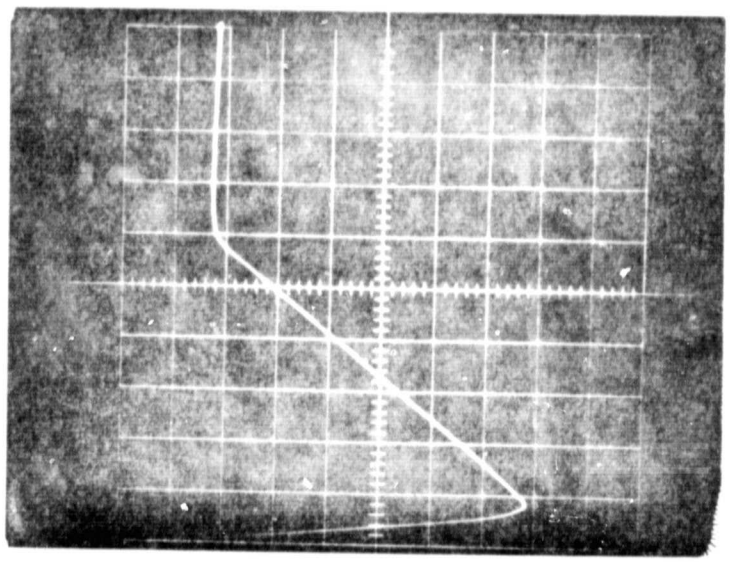

Figure 19. The V-I Characteristic of the NIC with Resistive Loading

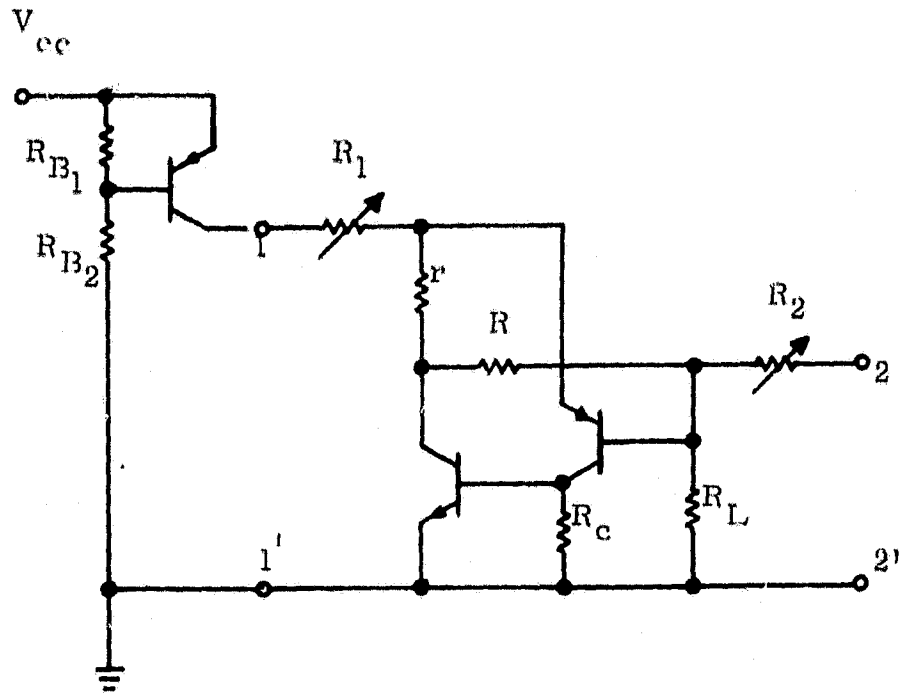

Figure 20. Constant Current Source Plus NII

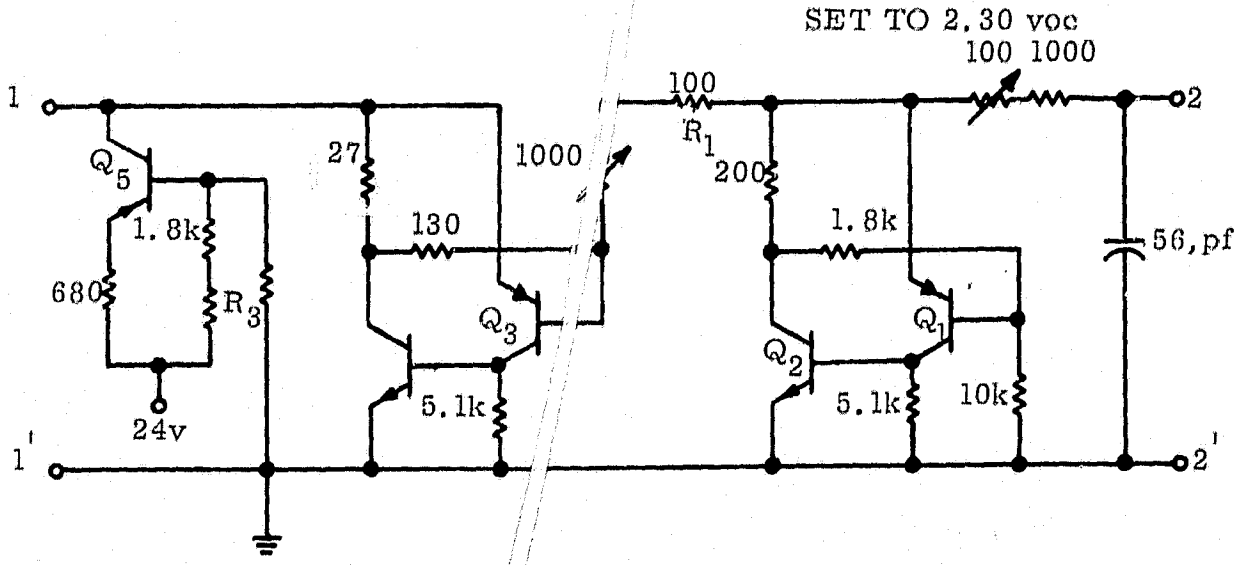

Figure 21. Final Circuit of Gyrator

N71-37801

SECTION II

Metallurgical Studies of Microcircuit Interconnections

Welville B. Nowak (Principal Investigator)
Thomas Hull
Peter Salmon

ABSTRACT

The behavior of vacuum evaporated films of Au, Pt, and Au-on-Pt, on glass substrates was observed after various heat treatments. Film thicknesses were 250 to 1800 Å and 4000 to 9000 Å for the Pt and Au, respectively. Heat treatment schedules were: (1) one hour in air at temperature intervals of 50°C from 100° to 650°C, or (2) increments of one hour, up to a total of seven hours, at 675°C in air. Room temperature electrical resistivity and spectral reflectivity (over the visible band) indicated the following: (a) Pt films appear to recrystallize when heated above 350°C, (b) Au-on-Pt couples blister when heated above 100°C, (c) an upper limit for the diffusion constant of the solubility phase boundary of Au in Pt at 675°C appears to be $D = 3 \times 10^{-16}$ cm^2/sec.

SECTION II

Metallurgical Studies of Microcircuit Interconnections

Welville B. Nowak (Principal Investigator)
Thomas Hull
Peter Salmon

I. Introduction

A. Background

Metal films are used for interconnection paths and supporting (beam) leads in integrated circuits. Aluminum is successfully and conveniently used in many cases. In other cases, multilayers of different metals must be used in order to meet complex requirements.[1-4]

Some of the failure modes of microcircuits are attributable to deterioration of the interconnection paths as manifested by

1. increased electrical resistance of the paths,
2. open paths
3. loss of adhesion between path and substrate.

Failure mechanisms include diffusion, chemical reaction, electromigration, and stress relief. Of particular interest in this investigation is diffusion.

It is well known that diffusion may sometimes proceed faster in films than in bulk material, presumably because of the greater density of defects (including grain boundaries)in films. This knowledge is often qualitative for two reasons: (1) the structural nature of films varies widely depending upon their fabrication processes, and (2) analysis of the diffusion is difficult. There is a need to measure interdiffusion in multilayer metal films and interactions between films and substrates as a function of film character and as a function of interaction time and temperature in appropriate environments (such as air, water vapor, and radiation or particle flux). These measurements will contribute towards an understanding of the observed phenomena and an ability to predict failure rates in a given environment. Logical steps may then be taken to reduce failures by changes in materials, design, or processing.

B. Objective of Program

The objective of this program is to measure quantitatively the interdiffusion between certain metallic films. Emphasis will be placed on laminated films and on substrates of practical importance, The purpose for undertaking this program is not only to fill gaps in our technical knowledge of thin film behavior, but to lead to improvements in the reliability and predictability of integrated circuits of particular importance to NASA.

C. Approach

The difficulties in obtaining diffusion (concentration) profiles in thin films reside in (1) the chemical analysis of very thin sections (layers), and (2) the removal and thickness determination of these very thin sections.

The first difficulty may be circumvented by using optical spectral-reflectivity. The second difficulty might be circumvented either by lapping the specimen at a small angle and analyzing it optically at high magnification, or by removal of thin sections (chemically or by sputtering) and analyzing optically with section thickness determined interferometrically.

We have reported[5] that a literature search revealed less than a dozen papers concerning thin film diffusion, and that the reflectivity technique was indeed a useful tool[6-10] in this field. In certain cases, very rapid initial diffusion was noted, but for the most part activation energies and diffusion constants were comparable to bulk material.[7-10] We also reported[5] our unsuccessful efforts at sectioning by angle-lapping and sputter-etching.

In view of the above, our approach in the work reported here was to utilize spectral reflectivity over the visible band at the surfaces of the film couples to provide an index of the concentration at (or near to) the surface. Efforts to obtain a concentration profile in the film were abandoned.

We chose the practical system of Au on Pt on glass for the investigations.

II. Experimental Details

A. Sample Fabrication

All of the data described in this report were obtained on samples prepared at the Bell Telephone Laboratories, Andover, Massachusetts, through the auspices of Mr. Thomas Hull. (Mr. Hull carried out much of the work reported here as partial fulfillment of the requirements for a Master of Science Degree at Northeastern University on the cooperative work-study plan.)

These samples were Au-on-Pt thin film couples deposited on Corning 7059 alumino-borosilicate glass microscope slides, 1" x 3", by thermal evaporation from tungsten filaments at about 10^{-5} torr. The glass substrates were held at 200°C for the Pt deposition and were allowed to cool to ambient temperature for the Au deposition (to inhibit diffusion during the evaporation procedures). Regions of pure Au and pure Pt were also deposited on the same substrate and in the same pump-down cycle as the Au/Pt couples by means of a spring-loaded two-position mask. These single-metal regions were used for electrical resistivity, optical reflectivity, and film thickness comparisons.

The glass substrates have a low coefficient of thermal expansion (4.5 ppm/°C), high electrical resistivity (10^{12} Ω-cm at 300°C), and good aging properties.[11] Each substrate was cleaned as follows:

1. Rinse in trichloroethylene,
2. Vapor degrease in trichloroethylene vapor, 10 min.,
3. Ultrasonic clean - 1:5000 solution of igepal and distilled deionized water at 150°F,
4. Rinse in hot, flowing deionized water, 5 min.,
5. Rinse in boiling hydrogen peroxide solution (3%), 10 min.,
6. Rinse in hot deionized water, 5 min.,
7. Rinse in hot, flowing distilled-deionized water until water resistivity reaches 8 megohms.

8. Oven dry in air at 100°C, 10 min.

The substrates were placed in the vacuum system and baked at 300-350°C for at least one hour before reducing their temperature to 200°C for the Pt deposition.

The evaporation rates were 400-600 Å/min and 3000-4000 Å/min for the Pt and Au, respectively.

Platinum and gold film thicknesses ranged from 250 to 1800 Å and from 4000 to 9000Å, respectively. In all cases, the gold was at least four times as thick as the platinum. Thicker Pt films were difficult to achieve using thermal evaporation from tungsten filaments. Unsuccessful attempts at thicker Pt films were also made from the following: tantalum filaments, tungsten coils with a boron nitride liner, and from tantalum baskets that were given a TaC coating. Very successful films were obtained using electron beam evaporation.

B. Measurement Techniques

Spectral reflectance was measured at normal incidence and at room temperature by directing monochromatic light into a metallurgical microscope (with the film specimen on the stage) and detecting the light output of the microscope eyepiece with a silicon solar cell.

The monochromatic light was achieved by filtering the output of a 1000 watt tungsten-iodide lamp (operated at about 750 watts). A Corning CS1-56 glass infrared filter, or about 1/2 inch of a 2% $CuCl_2$ solution, was placed between the lamp and one of the following filters:

Filter	Dominant Wavelength Passed (Å)
Wratten 70	6780
Corning Red	6330
Wratten 72B	6060
Wratten 73	5760
Wratten 74	5380
Wratten 75	4900

Absolute reflectivities of our films were obtained using fresh MgO standards, and were compared with literature values. Agreement to about ±10% was obtained. The reproducibility (precision) of our reflectivity measurements is a few percent. During the course of the work with the MgO standards it was found that they degraded in our laboratory environment over a period of several days. Fresh MgO standards had to be prepared for each day's reflectivity measurements. Another problem with these MgO standards was their lack of cohesiveness, so that they could not be used in the inverted position to obtain calibrations through the glass slide (substrate). These considerations led to the use of Eastman Kodak "white reflectance paint" (Catalog No. 6080, lot No. 1458) which is stable in air, very cohesive and durable, and is "white" for $350 < \lambda < 800$ millimicrons. This paint was used in all our calibrations to "correct" for the spectral absorption response of the optical system and detector. For most measurements, however, it was more convenient to use as a secondary standard an aluminum film (whose spectral reflectance is fairly flat over the visible band).

The current output of the solar cell detector was taken to be proportional to the reflected light from the sample. The current was measured with a Hewlett-Packard 425A pico-ammeter on the 300 nano-ampere scale.

The solar cell was placed close to the microscope eyepiece so as to intercept all the exit illumination. The cell was shielded from ambient light; and the connections from the cell to the meter were electrically shielded.

Film electrical resistivity was measured with a four-point probe, commonly used for semiconductors. The contact pins were spaced at 0.50 inch, and the current was constant at 5 milliamperes.

Film thickness was measured with a Talysurf 4 profilometer or with an interference objective attached to a microscope. The profilometer was used with a stylus diameter of 0.0001 inch and a load of 0.1 gram force.

III. Results and Discussion

The diffusion samples were relatively free of pin-holes, thus minimizing the error due to local diffusion at the boundary of the pin-holes. Adherence of the film to the glass was adequate, but not extremely good.

After annealing in air, even at 100°C for one hour, the presence of small blisters was noted, but only in the regions of the Au-on-Pt couples. Annealing for longer times, or at higher temperatures (to 675°C) resulted in an increase in the size of the blisters to approximately 0.07 cm in diameter. Examination of the Au side of a blistered film by reflection electron diffraction indicated that there were areas of single crystal Au, roughly the same diameter as the blisters, which were separated by areas of polycrystalline material. An explanation of this result may be the formation of curved, single crystal grains as diffusion progressed, similar to the effect in diffusion of single crystal films of Ni-Pd.[12] On the other hand, the blistering is doubtless connected with differing states of stress and differing coefficients of thermal expansion of the separate metals in the Au/Pt couple; and a strain-anneal crystal growth mechanism may be at work here.

In order to inhibit the blistering, and improve the adhesion, a thin layer of tantalum oxide was put on the glass slide. To do this, a thin film (about 500 Å thick) of Ta was sputtered onto the slide and then oxidized by heating the slide in air at 540°C for 22 hours. Then the Pt and Au films were deposited. Samples with the tantalum oxide film exhibited only slightly less blistering than those without the oxide.

An exploratory series of heat treatments was made on sample 2B, which had Au and Pt thicknesses of 5500 and 357 Å, respectively. The sample was heated in air for one hour at temperature intervals of 50°C, starting at 100°C and ending at 650°C. The corrected reflectivities of the Au and Pt films and the Pt side of the couple are plotted in Fig. 1 versus the temperature of the most recent annealing interval. Note that after annealing

at 350°C, the Pt reflectivities increase markedly. The Au reflectivity drops slowly as the temperature increases until 550°C, after which it drops rapidly (the Au may be diffusing into the glass).

Three samples, 5B, 5C, and 5D, with Pt thicknesses of 650, 450, and 260 Å, respectively, and Au thicknesses of 4000-6000 Å, were annealed at 657°C for increments of one hour up to a total of seven hours. The corrected reflectivities of the platinum side of the couples (measured through the glass slide) are plotted versus wavelength for the various annealing times in Figs. 2-7, inclusive. The initial similarity of the curves prior to annealing was lost after one hour at 675°C. No general trend was established after that.

The 5C Pt standard, Fig. 8, exhibited a rapid change in the magnitude of the reflectivity after one hour at 675°C. After three hours, the reflectivity-wavelength curve remained substantially constant. On the other hand, the 5C Au standard, Fig. 9, showed only a slight decrease in magnitude, reaching steady-state after two hours of annealing.

A final experiment was performed on sample 4C to verify the previous results. This sample had a Pt film of 1250 Å and a gold film of 5500 Å. After measuring the initial electrical resistivity and initial reflectivity at 4900 Å, the sample was annealed in air for one hour at 675°C. The results are given below:

Film Specimen	Reflectivity (4900Å) (Arbitrary Units)		Electrical Resistivity (25°C) (microhm-cm)		
	Initial	Final	Initial	Final	Bulk
Au	290	250	2.7	2.7	2.44
Pt	62	152	90	20.3	10.5
Pt side of Au/Pt	60	200	--	--	

The electrical resistivity values in the above Table are typical of the films reported here, and they indicate that the films contained many defects, especially the Pt films.

It is worth remarking that although the thin Pt films were not optically opaque, the reflectivity of the Pt film through the glass matched that of the Pt in the Pt/Au couple. This result is supported by the theoretical curve for Pt reflectivity versus film thickness that appears in reference 13.

One might guess that the increase in reflectivity and decrease in resistivity of the Pt films are caused by a recrystallization of the film, even at this low temperature.

Since the expected changes in reflectivity did not occur until after seven hours at 675°C, an upper limit for the effective diffusion constant of the solubility phase boundary of Au in Pt at 675°C may be computed from the relation $x^2 = Dt$. This upper limit is $D \simeq 3 \times 10^{-16}$ cm^2/sec.

Several models for diffusion in thin films are available in the literature. In addition to models proposed by Schopper, and by Weaver and Brown, one may derive another one by analogy to the heat transfer in a finite slab. The following derivation is taken from the M.S. thesis of Thomas Hull.

The solution to the finite slab with insulated faces and initial temperature distribution is taken from Carslaw and Jaeger.[14]

$$v = \frac{1}{L}\int_o^L f(x')dx + \frac{2}{L}\sum_{n=1}^{\infty}\left[e^{-\frac{kn^2\pi^2t}{L^2}}\cos\frac{n\pi x}{L}\int_o^L f'(x)\cos\frac{n\pi x'}{L}dx'\right]$$

where $f(x')$ = initial temperature distribution

v = temperature

L = total thickness

k = heat transfer coefficient

t = time.

The diffusion analogy is:

$$C = \frac{1}{L}\int_o^L f(x')dx + \frac{2}{L}\sum_{n=1}^{\infty}\left[e^{-\frac{Dn^2\pi^2t}{L^2}}\cos\frac{n\pi x}{L}\int_o^L f(x')\cos\frac{n\pi x'}{L}dx'\right]$$

where C = composition

D = diffusion constant.

To approximate the multicomponent film, the initial distribution is:

$$f(x') = C_o, \qquad 0 < x < h$$

$$f(x') = 0, \qquad h < x < L$$

Thus, the integrals become:

$$\int_o^L f(x')dx = \int_o^h C_o dx' + 0 = hC_o$$

and

$$\int_o^L f(x')\cos\frac{n\pi x'}{L}dx' = \int_o^h C_o\cos\frac{n\pi x'}{L}dx' + 0 = \frac{C_oL}{n\pi}\sin\frac{n\pi h}{L}$$

The solution becomes:

$$C = \frac{hC_o}{L} + \frac{2C_o}{\pi} \sum_{n=1}^{\infty} \left[\frac{1}{n} e^{-\frac{Dn^2\pi^2 t}{L^2}} \cos\frac{n\pi x}{L} \sin\frac{n\pi h}{L}\right]$$

$$\frac{C}{C_o} = \frac{h}{L} + \frac{2}{\pi} \sum_{n=1}^{\infty} \left[\frac{1}{n} e^{-\frac{Dn^2\pi^2 t}{L^2}} \cos\frac{n\pi x}{L} \sin\frac{n\pi h}{L}\right.$$

If we consider a surface analysis, then:

$$x = 0$$

and the solution reduces to:

$$\frac{C}{C_o} = \frac{h}{L} + \frac{2}{\pi} \sum_{n=1}^{\infty} \frac{1}{n} e^{-\frac{Dn^2\pi^2 t}{L^2}} \sin\frac{n\pi h}{L}$$

IV. Conclusions

Platinum films deposited onto glass substrates at 200°C by vacuum evaporation appear to recrystallize when subsequently heated above 350°C.

Adhesion of gold-on-platinum bilayer films on glass substrates is much poorer than either gold or platinum single films upon heating to temperatures over 100°C. Evidence for poor adhesion is blistering of the films. A thin tantalum oxide layer put on the glass before the platinum deposition reduces the blistering.

On the basis of the exploratory experiments reported here, it seems that the diffusion constant of the solubility phase boundary of gold in platinum at 675°C has an upper limit of $D = 3 \times 10^{-16}$ cm^2/sec.

It is evident that if gold-on-platinum films for microcircuit interconnections are prepared in a fashion similar to that reported here, failures may be encountered because of lack of adhesion to the substrate if the microcircuit is subjected to temperatures over 100°C. It is not known whether the changes in the platinum film on heating above 350°C would lead to electronic failures, but it is a phenomenon worth keeping in mind. Possible failures due to the diffusion of gold through the platinum do not appear likely in view of the probable low value for the diffusion constant.

V. References

1. W. M. Berger, R. S. Keen, G. L. Schnable in "Physics of Failure in Electronics," Vol. 4, 1966 Report No. 637529, Defense Documentation Center, Alexandria, Virginia 22314.

2. "Advanced Technology of Interconnections in Microelectronics," May, 1967, Interim Scientific Report prepared by Motorola, Inc. for the National Aeronautics and Space Administration, Electronics Research Center, Cambridge, Massachusetts under Contract No. NAS 12-132.

3. W. H. Gianelle in "Physics of Failure in Electronics," Bol. 4, 1966, Defense Documentation Center Report No. 637529.

4. J. A. Cunningham, Solid State Electronics, 8, 735 (1965).

5. Welville B. Nowak, "Metallurgical Studies of Microcircuit Interconnections," Section II of Final Report, 1 January 1969, on NASA Research Grant NGR-229011-007.

6. H. Schopper, Zeit. f. Phys., 143, 93 (1955).

7. C. Weaver and R. M. Hill, Advances in Physics, 8, 375 (1959).

8. C. Weaver and L. C. Brown, Phil. Mag., 7, 1 (1962).

9. C. Weaver and L. C. Brown, Phil. Mag., 8, 1379 (1963).

10. C. Weaver and L. C. Brown, Phil. Mag., 17, 881 (1968)

11. R. Berry, P. Hall, M.T. Harris, Thin Film Technology,D. Van Nostrand Co., Princeton, N.J., 1968, p. 706.

12. J. W. Matthews and W. A. Jesser, J. Vac. Sci. & Technology, 6, 641 (1969).

13. O. S. Heavens, Optical Properties of Thin Solid Films, Dover Pub. Co., New York, 1965, p. 261.

14. H. S. Carslaw and J. C. Jaeger, Conduction of Heat in Solids, Clarendon Press, Oxford University, England, 1959, p.101.

VI. Acknowledgements

The help and advice of James Surette in conducting the laboratory work is gratefully acknowledged.

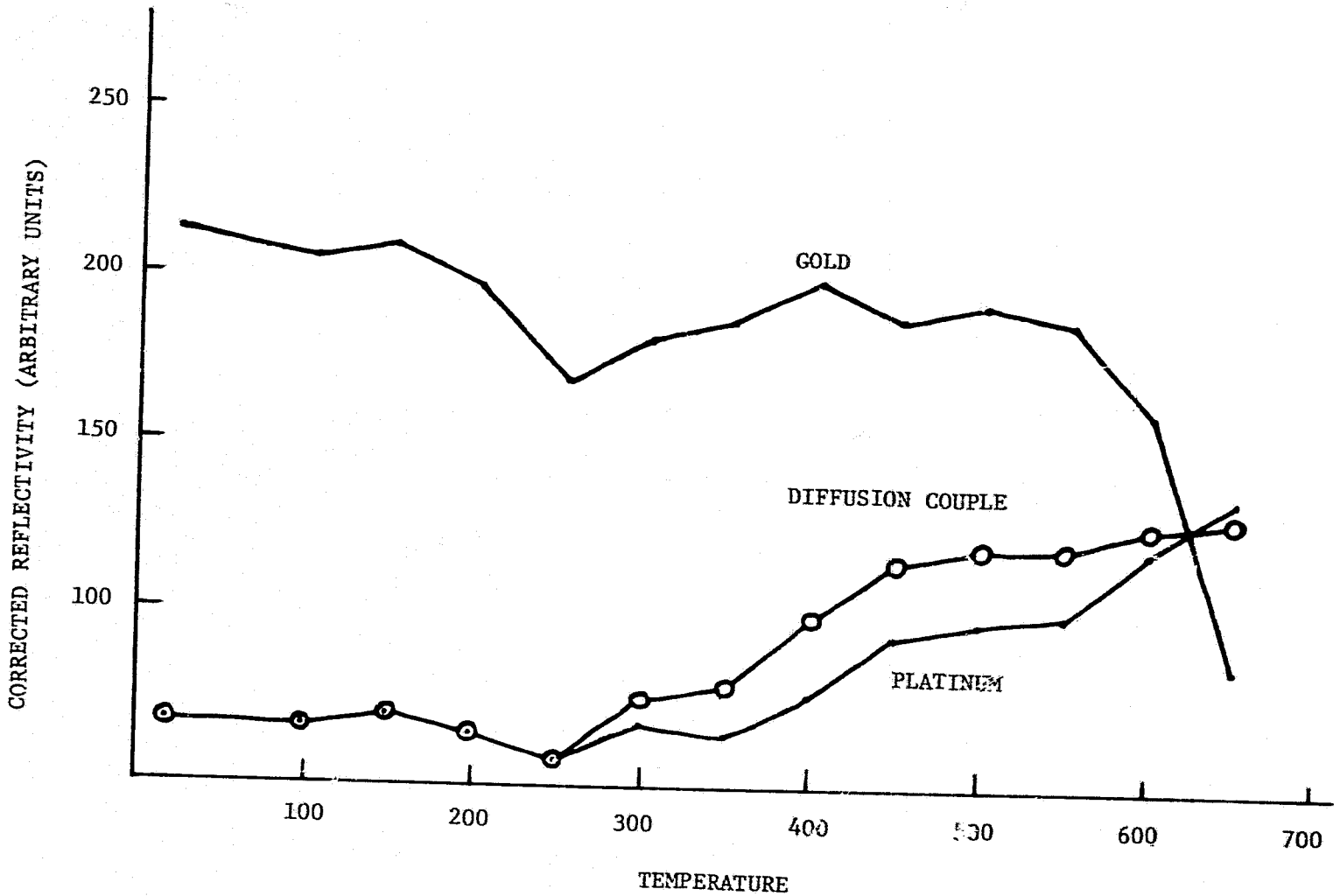

Fig. 1: Reflectivity vs. annealing temperature. Annealed for 1 hour at each progressively higher temperature. λ = 6780 Å. (Sample 2B)

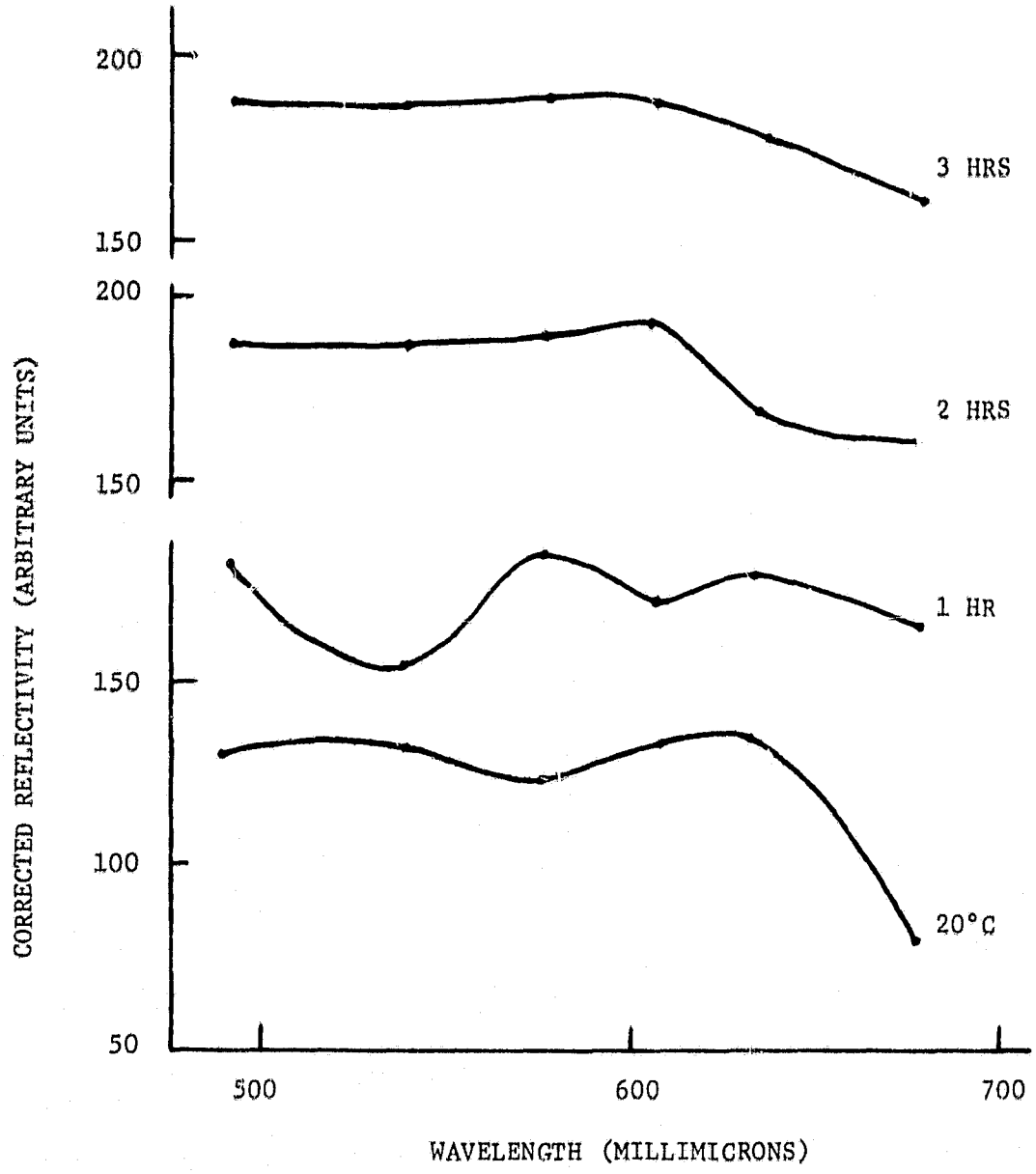

Fig. 2: Platinum reflectivity vs. wavelength for annealing times at 675°C. (Sample 5B)

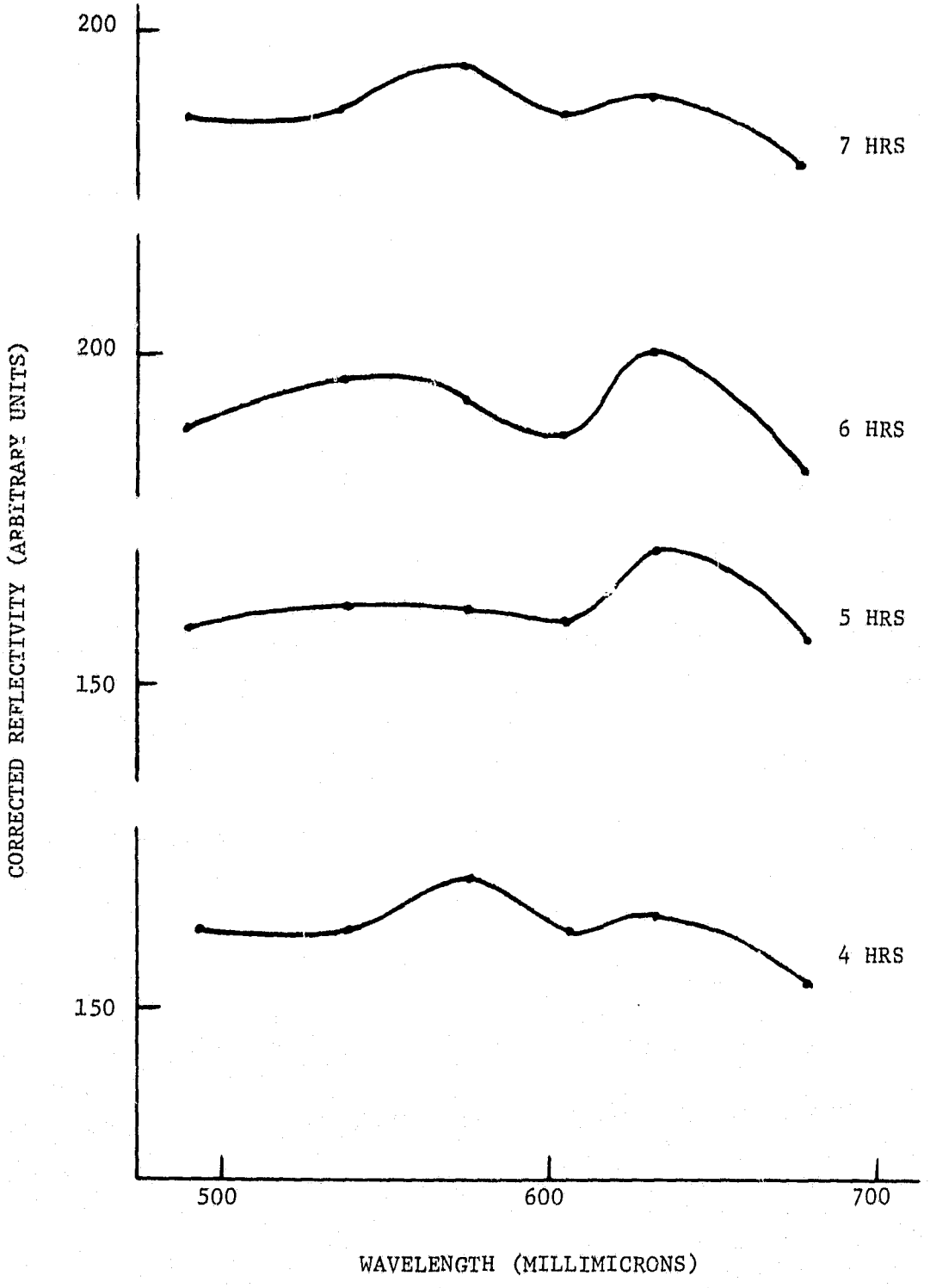

Fig. 3: Platinum reflectivity vs. wavelength for annealing times at 675°C. (Sample 5B)

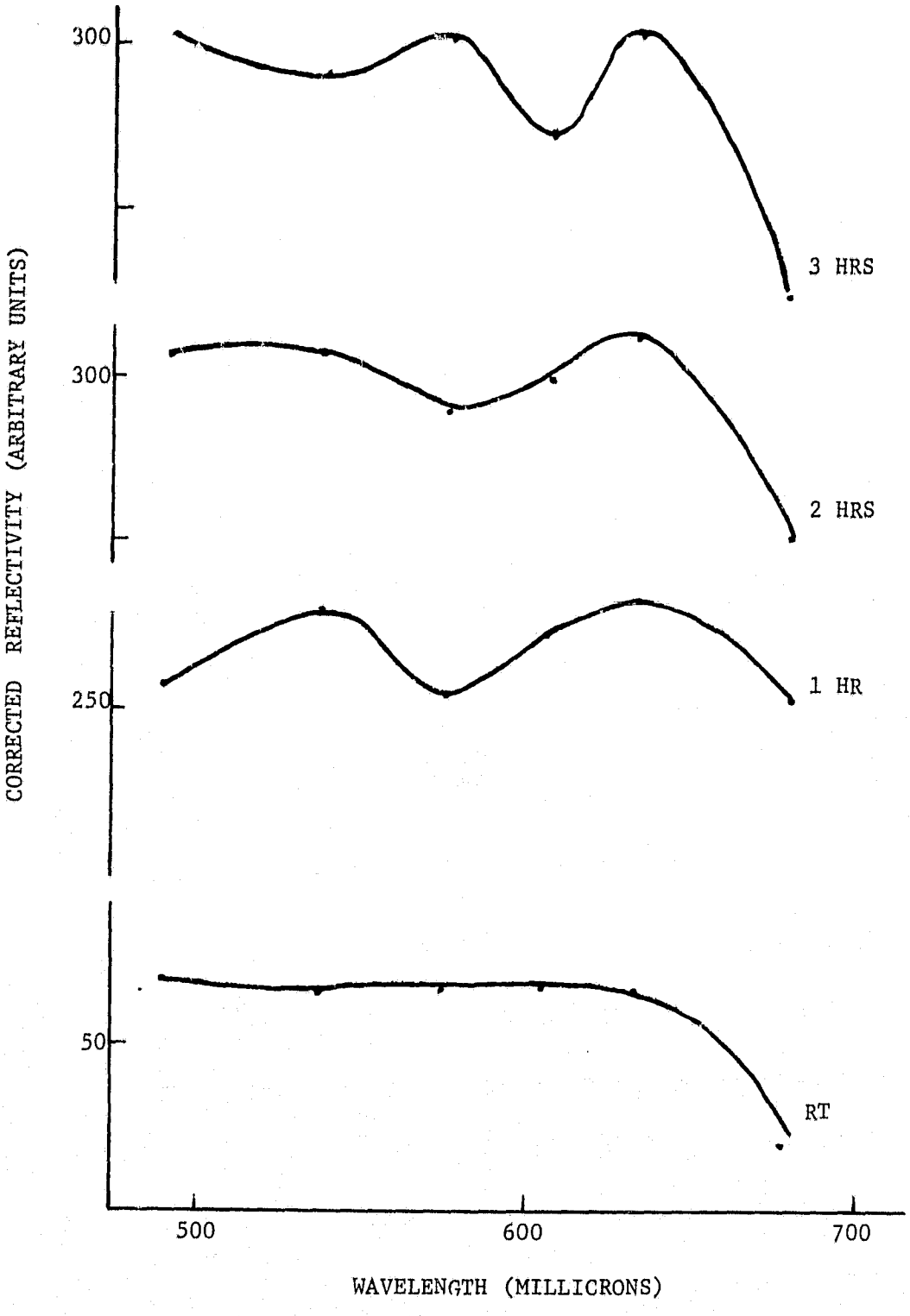

Fig. 4: Platinum reflectivity vs. wavelength for annealing times at 675°C. (Sample 5C)

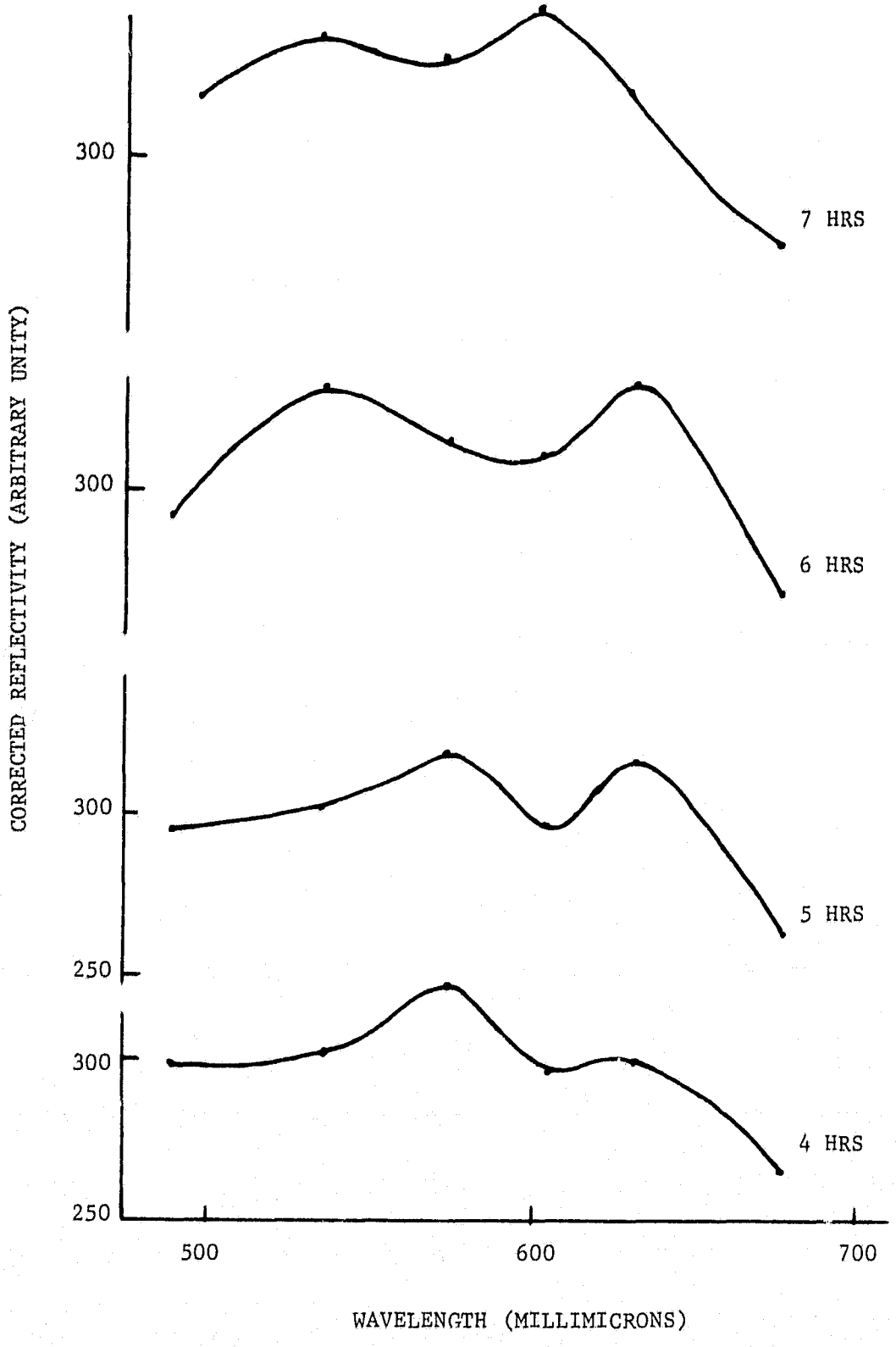

Fig. 5: Platinum reflectivity vs. wavelength for annealing times at 675°C. (Sample 5C)

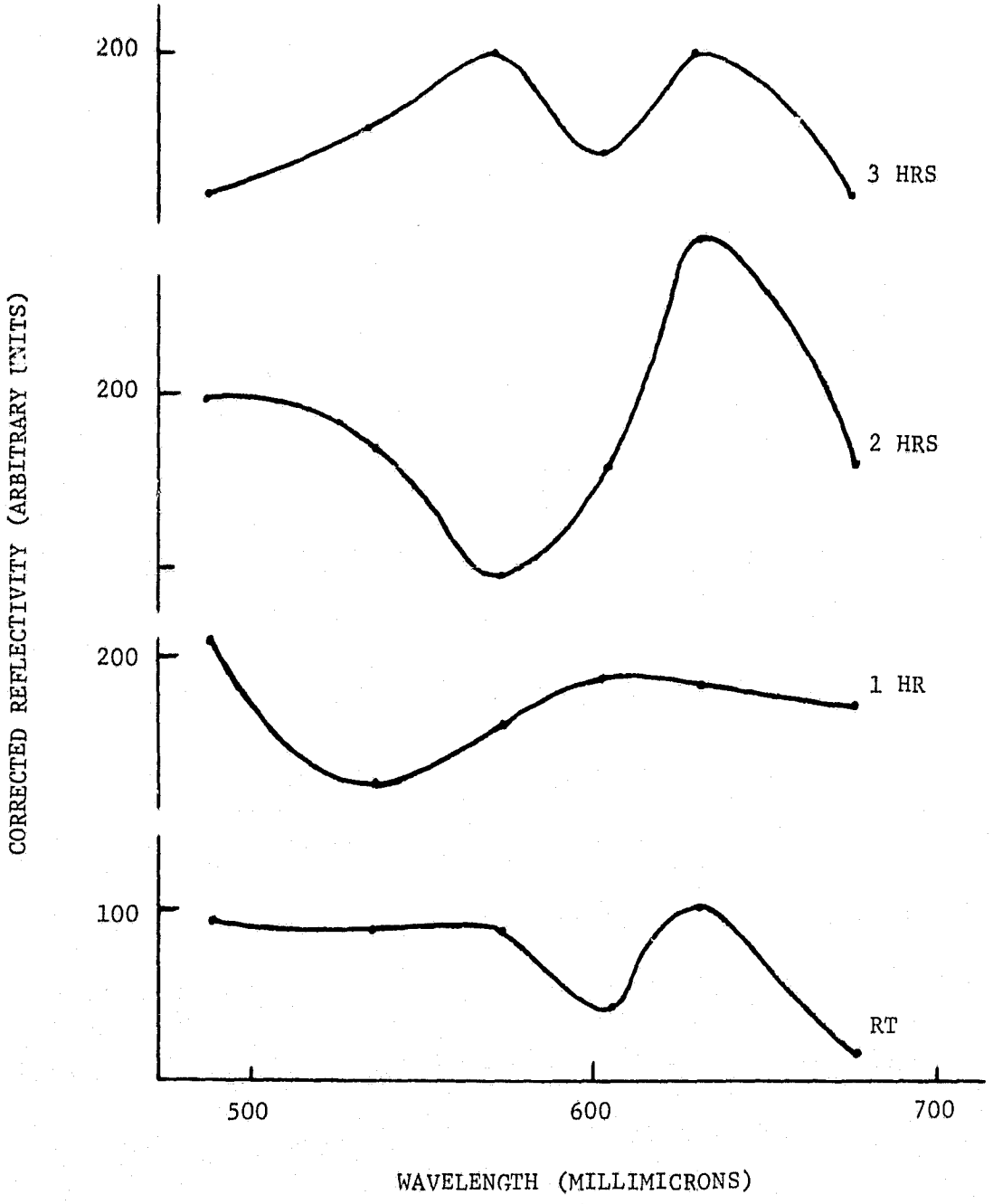

Fig. 6: Platinum reflectivity vs. wavelength for annealing times at 675°C. (Sample 5D)

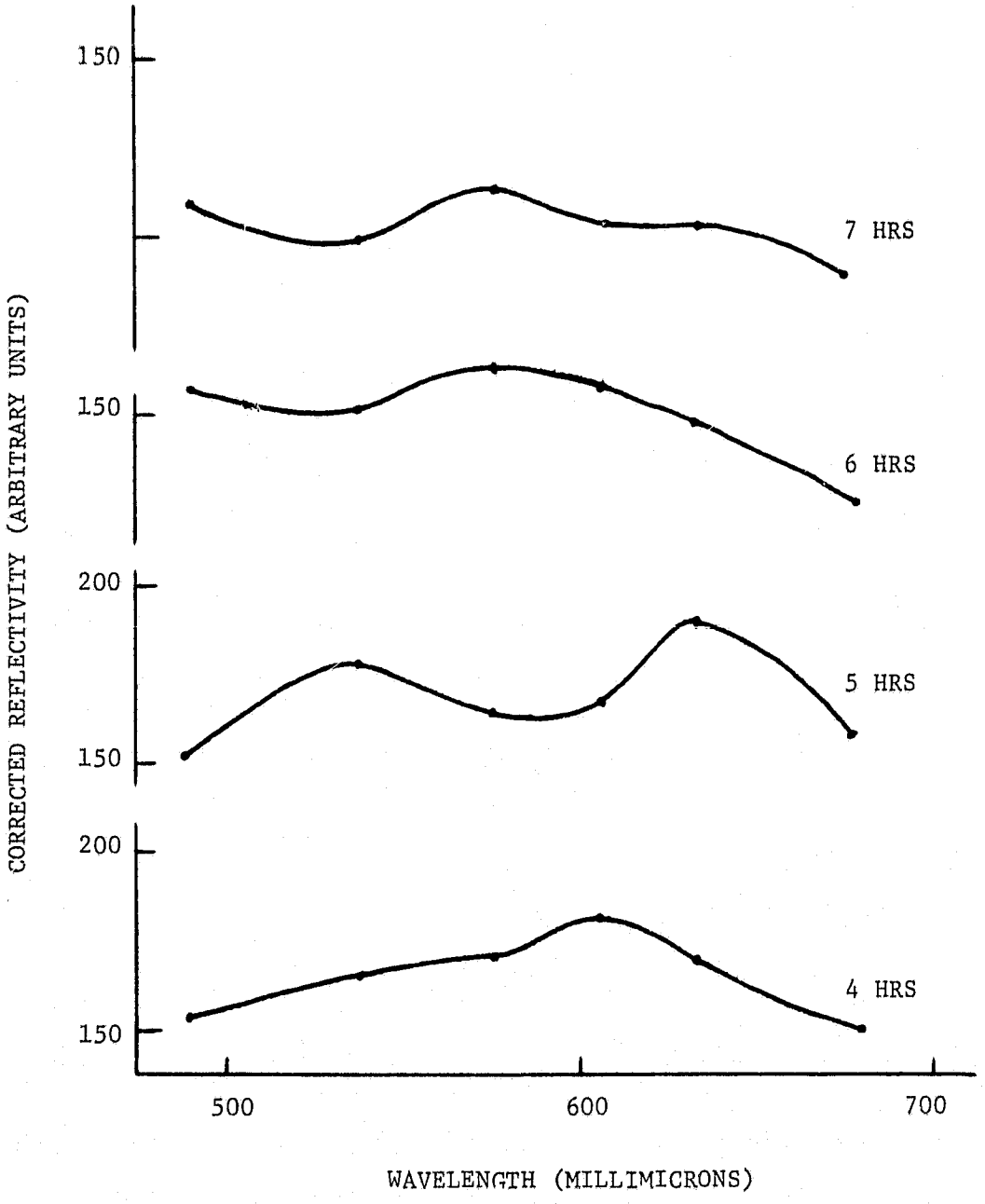

Fig. 7: Platinum reflectivity vs. wavelength for annealing times at 675°C. (Sample 5D)

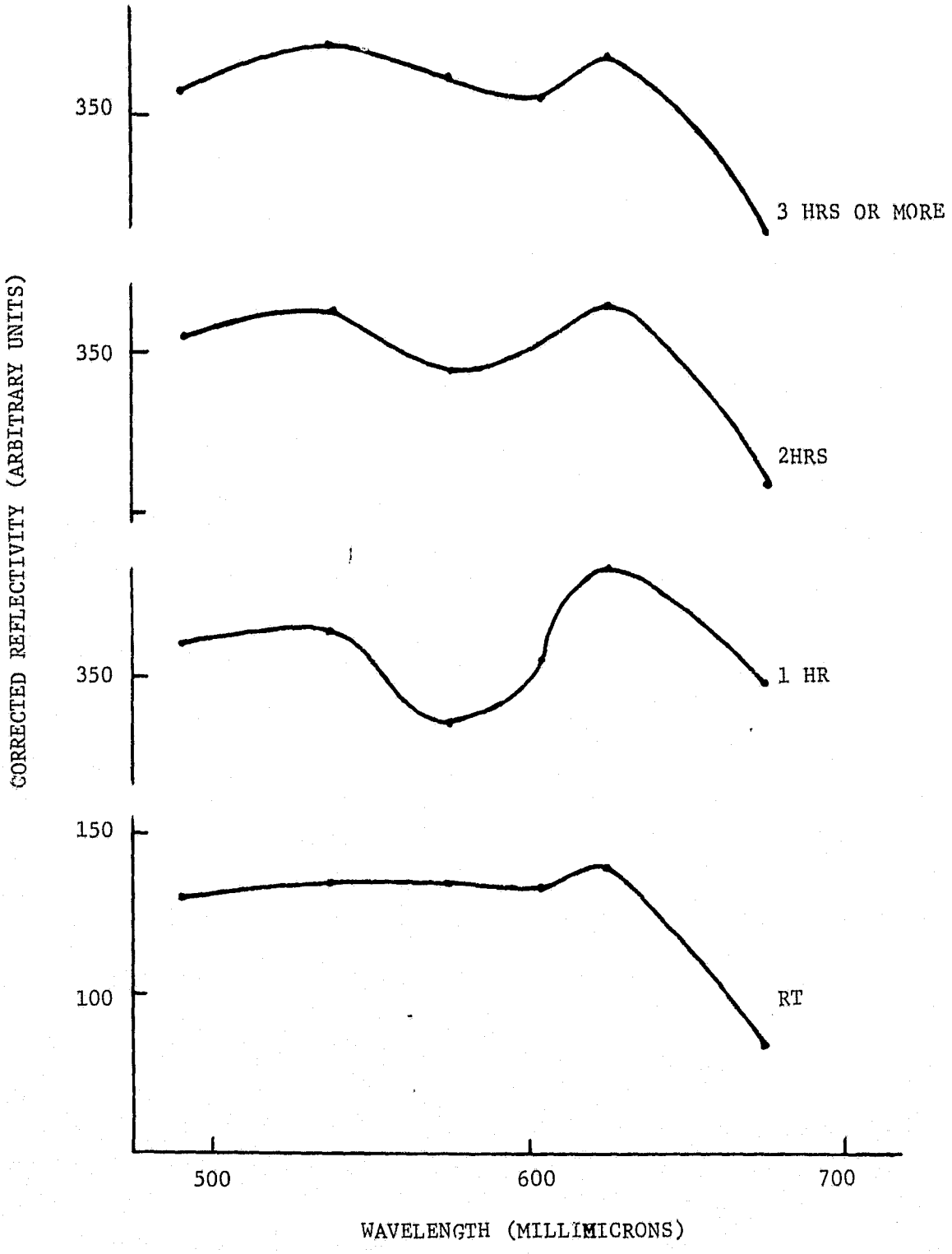

Fig. 8: Reflectivity vs. wavelength for 5C platinum standard. Annealed at 675°C.

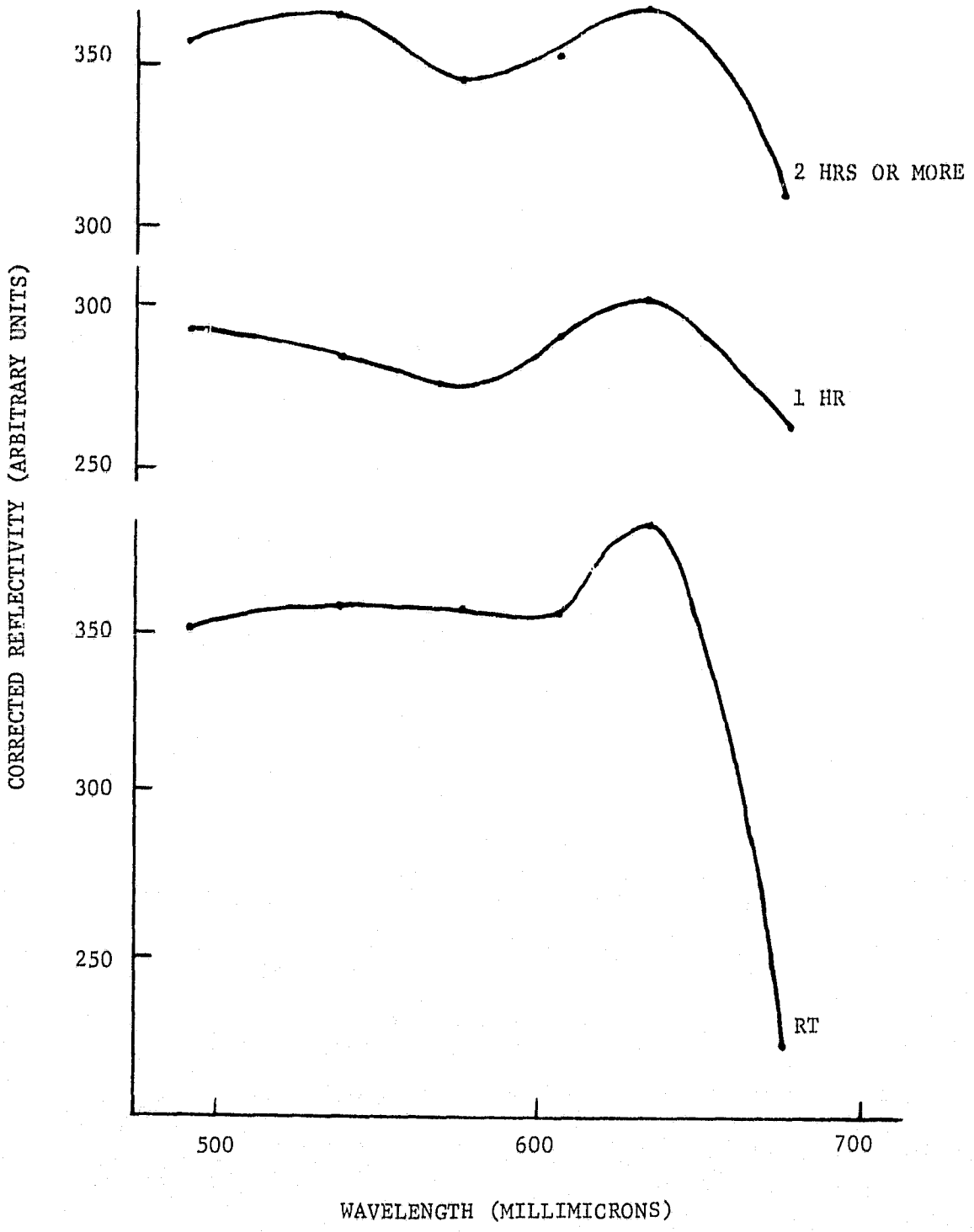

Fig. 9: Reflectivity vs. wavelength for 5C gold standard. Annealed at 675°C.

N71-37800

SECTION III

Biophysical Studies

b. Fine

The National Aeronautics and Space Administration is involved in a number of projects which require the use of lasers at a number of wavelengths, power and energy levels. In many of these studies it is necessary to know the thresholds for injury at the laser wavelength used in order that adequate precautions can be taken to minimize the hazard. Thus the operational capabilities of the laser system can be optimized. Furthermore, with the increasing use of lasers, information regarding the effects of threshold and suprathreshold radiation, on both a short and long term basis, is important to the civilian populace in order to permit assessment of the degree of injury and to allow consideration to be given to meaningful methods of therapy, should accidental injury occur.

Another area of interest to the National Aeronautics and Space Administration is the application of knowledge and understanding gained through in-house research and through extramural grants and contracts to areas of biology and medicine, so as to improve medical care both on a national and on an international basis.

Consequently, some of the effort supported in part by this contract during this past period have been devoted to assessing and delineating some of the hazards associated with laser radiation of specific characteristics and determining methods in which laser radiation can be used as a tool in biology and medicine. The results obtained will be of value to the country as a whole with regard to delineation and minimization of laser hazards and to medicine and biology where lasers are used as a tool.

The following is, therefore, an outline of the laser related areas which have been supported in part by this contract.

1. "Toxic and Explosive Hazards Associated with Lasers," D. MacKeen, S. Fine, and E. Klein, published in Laser Focus, pp. 47-49, October 1968.

In this publication, consideration is given to hazards associated with ancillary materials as well as with the active laser media. These could be encountered either during manufacture of the equipment or during its use. Elements and compounds presently used whether in the manufacture of the equipment or in conjunction with their operation were divided into six groups. The scope of each group extended from the relatively innocuous to the extremely hazardous. The value of this report is that it should alert the industry, including NASA contractors, to potential chemical and toxic hazards which may arise. Some safety procedures which can be initiated are recommended.

2. "Application of Thermal Models to Retinal Threshold Injury," W. P. Hansen and S. Fine, presented at the Laser Industry Association Meeting, October 24-26, Washington, D. C., published in Proceedings of Conference, 1969.

Helium neon lasers are in common use at NASA as well as throughout the country. In this report, analytical techniques were described for estimating the maximal retinal temperature elevation occurring during a step input of laser power to a retinal image of given size. It was shown that for a 10 micron retinal image diameter, the maximum temperature elevation cannot be limited by a voluntary avoidance reaction on the part of the observer. Thus, the hazards involved in the use of He-Ne (and similar) lasers has been more clearly delineated than previously. This is of interest to NASA, its contractors and to the civilian populace as a whole.

3. "Exploration of Potential Carcinogenic Effects of Pulsed Laser Radiation," F. Bock, Y. Laor, S. Fine, and E. Klein, presented at the Laser Industry Association meeting, October 24-26, Washington, D. C., published in Proceedings of Conference, 1969.

There is a greater propensity for malignant transformation following burns of the skin. Since pulsed laser radiation as produced with ruby lasers produces a burn as well as possibly other effects, investigations of the potential for production of cancer following ruby laser radiation is of significance. Long term studies of the tendency for malignant transformation following pulsed laser irradiation with and without a co-carginogen were consequently carried out on mice. The results to date have not shown any

significant increase in the rate of tumor formation following pulsed ruby laser irradiation. It should, however, be understood that extrapolation of this data to man is, of course, difficult since as is well known there are species differences for malignant transformations. The studies should, however, at least provide some guidelines for follow-up in the case of accidental injury or where lasers are employed as a therapeutic modality.

4. "Anterior Chamber Measurements on CO_2 Laser Corneal Irradiation," S. Fine, D. MacKeen, L. Feigen, and B. S. Fine, published in Proceedings of the Annual Conference on Engineering in Medicine and Biology, Vol. 10, November 1968.

Previous studies have shown that anterior indentation of the lens occurs on fixation in gluteraldehyde following suprathreshold rabbit corneal irradiation, without perforation of the cornea. In this report, the mechanism by which the lens alteration occurs was examined. It was shown that increased pressures and temperatures are produced in the anterior aqueous chamber. Above a certain temperature-pressure level, alterations in the lens of the eye could be produced which on fixation resulted in indentation. Below this level, indentation did not occur. Coincident with the changes in the anterior chamber, flattening of the cornea occurred, thus bringing this "secondary heat source" into closer approximation to the lens. These alterations in the lens are of significance since they may affect the therapeutic procedures considered.

5. "Corneal Calcification," B. S. Fine, J. Berkov, and S. Fine, Science, Vol. 162, October 4, 1968, pp129-130.

In studies on the effects of continuous CO_2 laser irradiation of the cornea, a number of rabbit eyes developed clinical and histopathological changes identical with band keratopathy as observed in the human cornea. The calcification was entirely extracellular and characterized as hydroxyapatite by x-ray diffraction. The lesions, examined by electron microscopy, appeared as calcific spherules and conglomerates. The extra-cellular form of calcification obtained differed in morphologic features from the intracellular calcification that has been seen in hyperparathyroidism, but was similar to band keratopathy on humans.

The National Aeronautics and Space Administration is concerned with the properties and capabilities of biological systems, in particular human systems,

since these will affect man's ability to successfully undertake prolonged extraterrestial travel. Medicine is also concerned with the properties and capabilities of human systems. In some cases, various tissues are used as allografts, homografts or heterografts. Methods for sterilization and preservation of biological tissue are of importance to NASA and to medicine. Consequently, some attention has been directed to the area of investigation discussed below

6. "Rupture and Tensile Strength Measurements of Fresh and Treated Canine Aortic Tissue," S. B. Litwin, J. Cohen, S. Fine and A. Aaron, Proceedings of the Annual Conference on Engineering in Medicine and Biology, Vol. 10, November 1968.

Successive transverse sections of normal and treated canine aortas were cut to a standard size from the ascending aorta to the common iliac vessels. The aortas were sterilized with beta-propiolactone, or stored either in a graft bank at -70°C for 3 to 30 days or in a 4% buffered formaldehyde mixture for 1 to 19 days. Using an Instron test machine, specimen thickness, force-elongation curves, the maximum force for rupture and the tensile strength were obtained. The variation of rupture strength and tensile strength with position along the untreated aorta were determined and the effect of the treatment on rupture force and tensile strength assessed.

7. "Lasers in Biology and Medicine" S. Fine and E. Klein, Laser Focus, July 1969.

In this survey, attention was directed towards representative studies relating to lasers in biology and medicine. These areas included laser-microscope systems, applications in embryology, holographic microscopy, cell culture and macromolecular studies, studies on normal animals, animal tumor studies, and medical studies including the use of the laser in ophthalmology, urology, anesthesiology, as an aid to the blind, measurements of eye refraction and studies on protective glasses.

Some of these areas will be of interest to NASA, since they are concerned both with protection against laser radiation as well as possible utilization of advances in lasers for biological and medical purposes.

8. "Pathology of Internal Viscera Following Laser Radiation," Y. Laor, C. L. Simpson, E. Klein and S. Fine, Am J. Medical Sciences, Vol 257, April 1969.

This discusses some of the changes which take place on laser irradiation of internal organs. The pathology observed may provide some information pertinent to laser radiation interaction in man, either accidental or deliberate for medical purposes.

9. "A Method for Detecting and Measuring Frequency of Surface Vibrations Using a Helium-Neon Laser", L. Feigen, D. MacKeen and S. Fine, the Review of Scientific Instruments Vol. 40, No. 2, 381-382, February 1969.

By chopping a laser beam at the same rate as the frequency of a mode of vibration of a surface, a stationary speckle pattern corresponding to that mode of vibration was observed. This study indicated that the speckle pattern might be of interest for studying modes of vibration or vibration patterns.

10. "Lasers in Biology and Medicine", S. Fine and E. Klein in Developments in Laser Technology Seminar Proceedings, Society of Photo-Optical Instrumentation Engineers, 1970.

In this survey, attention was directed to lasers for use in spectroscopic ultramicroanalysis, laser microscope studies, lasers in biophysics and biochemistry, laser studies on intact and tumor bearing animals and laser studies in medicine.

11. "Preliminary Report of Biological Testing of Laser Protective Materials" S. Fine, D. MacKeen, J. Berkow and B. S. Fine Am. J. Ophthalmology, Vol. 71, No. 4, April 1971

With the increasing use of systems incorporating lasers in scientific research and industry, the potential for accidental injury is increased. Ocular injury that can occur on such accidental exposure may frequently result in permanent loss of visual function. Such injury almost invariably leaves a demonstrable tissue alteration.

Attempts have been made to determine various thresholds of injury for some of the ocular tissues (e.g., retina, cornea) for several laser wavelengths (e.g., 694.3 nm, 1060 nm), and devices or materials have been developed to protect the eye. The required characteristics of such protective materials,

in particular the optical density (OD) at the laser wavelengths, have been based primarily on calculations and physical measurements (including direct irradiation of the material).

It seemed reasonable to use the eye as a sensitive biologic indicator for evaluating the efficiency with which these materials attenuate the laser radiation at relatively high levels of power density, since it is not known whether physical measurements alone can accurately predict the degree of safety offered by a specified material at a given optical density. At higher power levels unexpected injury might occur in spite of the use of a device calculated to afford adequate protection. The eye, in vivo, would also assist in determining whether injury to tissues other than the retina could occur when the eye is protected by safety material against laser irradiation.

A series of filters having considerable attenuation at the ruby laser wavelength were evaluated as protective devices for the eye in short-term studies by using the sensitivity of in vivo ocular tissue response. The ability of the filter to protect the eye increased with increasing optical density at the laser wavelength, as expected. Long-term studies are needed to evaluate possible delayed effects.

Compared with normal-mode irradiation, the relative hazard of Q-switched irradiation at suprathreshold levels is much greater than expected from threshold studies.

The use of multiple irradiations rather than single exposures to an eye with and without interposition of filters might provide a good criterion for establishing thresholds for injury as well as determining the degree of protection offered by laser protective glasses.

12. "Preventable hazard at UW Wavelengths" D. MacKeen, S. Fine, A. Aaron, and B. S. Fine

The increasing acceptance of the ultraviolet laser necessitates examination of hazards at wavelenths around 3,250 angstroms, with the objective of

alerting users rather than alarming them.

Preliminary studies showed that cataractous changes could be produced in a rabbit's eye after continuous, 16-minute exposure to a direct beam from a 10-milliwatt helium-cadmium laser. The primary sites of injury appear to be the lens and cornea rather than the retina, as with ruby helium-neon and neodymium lasers. No gross irreversible lesions were observed after two-minute irradiation.

It should be emphasized, however, that exposure of personnel to a direct beam for periods of minutes is all but inconceivable. Furthermore, simple and straightforward protective techniques are available to prevent ocular injury at these wavelengths.

Since NASA will be using ultraviolet lasers for a number of purposes, the hazards involved are of interest.

13. "Heat Sensation Thresholds for CO_2 Laser Radiation", J. Campbell, and S. Fine, Radiation Research, 43 (1): 1970.

CO_2 lasers are being used to an increasing extent in research and in systems. In this psychophysical study, reciprocity was shown to exist between reaction time and irradiance over a range of irradiances for production of heat sensation in two Caucasian males.

14. "Determination of Cardiac Output by Dye Dilution", A. Aaron S. B. Litwin, S. Fine and A. Rosenthal, Proceedings of the 23rd Annual Conference on Engineering in Medicine and Biology, Vol. 12, 1970

Comparative studies on cardiac output have been carried out with earclip versus withdrawal cuvette and with arterial cuvette versus electromagnetic flowmeter. The purpose of this study was to compare the three methods simultaneously on dogs.

The cardiac output as determined by the earclip cuvette agreed with the arterial cuvette determination within the experimental error. The earclip/arterial cuvette ratio (Paired samples) was 0.97 $\pm$ 0.12 SEM based on arterial

calibration samples. The ratio of earclip/electromagnetic flowmeter (paired samples) determination was 1.03± 0.11 SEM. The ratio of the standard dye dilution determination to the electromagnetic flowmeter determination (paired samples) was 1.03 ± 0.1 SEM. There was little difference in the dye concentration as measured in simultaneous samples at an arterial site and a venous sampling site in the inferior vena cava at the right atrium. There was a difference between the cardiac output as determined by sampling near the right atrium and sampling at the insertion of the hepatic vein. The sampling at the hepatic vein resulted in a cardiac output higher than that determined by the other two techniques. Presumably the reason for this is the loss of dye in the liver in conjunction with slow mixing at the outflow orifice of the hepatic vein.

Since there are alterations in cardiac output with stress these studies should be of interest to NASA with regard to accuracy of comparative methods of measurement of cardiac output, and identifying biases which would exist in the three methods, such as finite withdrawal rate in the cuvette method and calibration of the earclip.

15. "Optical Second Harmonic Generation in Biological Systems," S. Fine and W. P. Hansen, accepted for publication in Applied Optics, October 1971.

A Q-switched ruby laser was used to irradiate exiced biological tissues. An isolated narrow-band emission line was observed at 347 nm on irradiation of collagenous tissues. Temporal pulses at 347 nm were narrower than the laser pulses at 694 nm. Reduced crystalline glutathione yielded narrow-band emission at 347 nm that was similar to that for the collagenous tissues. The observed narrow-band emission at 347 nm is thought to be due to optical second harmonic generation.

The studies described in this report indicate that the cornea may produce visible second harmonic radiation when irradiated in the near-infrared (e.g., with neodymium or erbium lasers). The efficiency for SHG increases as the fundamental irradiance is increased. Thus it is possible that the threshold for visibility of a second harmonic lies below the threshold for injury to

the eye at the fundamental wavelength. Consequently, harmonic generation in ocular tissue may be of significance to vision.

Consequently, these studies relating to harmonic generation in the eye are of interest to NASA.

INVITED PRESENTATIONS DEPENDENT IN PART ON THIS CONTRACT

1. S. Fine - "Biological Studies on Laser Radiation, Particularly with Regard to the Eye," Howe Laboratories, Massachusetts Eye and Ear Infirmary, Harvard Medical School, Boston, Mass., December 1968.
2. S. Fine - "Control of Laser Hazards and Management of Accidents," National Center for Radiological Health, Rockville, Md., February 1969.
3. S. Fine - "The Application of Lasers in Biology and Medicine," Conference on Trends and Directions in Biological Sciences of the Thirteen Colleges Curriculum Program Biology Teachers, Clark College, Atlanta, Georgia, March 1969.
4. S. Fine - Participation in Skin Laser Workshop, Second International Laser Safety Conference, Cincinnati, Ohio, March 1969.
5. S. Fine - Lasers - Characteristics, Use, Hazards and Biological Effects, Seminar Series, Environmental Health Engineering and Science, Graduate School of Engineering, Northeastern University, March 1969.
6. S. Fine - Lasers - Characteristics and Uses in Biology and Medicine, Surgical Seminar Series, Boston University School of Medicine, March 1969.
7. S. Fine - Use of Lasers in Biology and Medicine, Laser Applications Course, Washington University, St. Louis, Missouri, May 1969.
8. E. Klein and S. Fine. - Tissue and Cell Effects of Laser Radiation - Gordon Research Conference on Lasers in Medicine and Biology, June 1969.
9. S. Fine - "Biological Hazards and Effects of Laser Radiation," in course on Fundamentals of Non-Ionizing Radiation Protection, Northeastern Radiological Health Laboratory, August 1969.
10. S. Fine - "Laser Biology" - in Laser Fundamentals and Applications course, Polytechnic Institute of Brooklyn Graduate Center, September 1969.
11. S. Fine and E. Klein - "Biological Effects of Laser Radiation," the Theobald Smith Society, New Jersey, October, 1969.
12. S. Fine - "Lasers - Biological Effects and Medical Applications," Society of Photo-Optical Instrumentation Engineers Meeting, co-sponsored by the University of Rochester Institute of Optics, Rochester, N.Y., November 1969.
13. S. Fine - Session Chairman - Laser and Ultraviolet Contributed Papers, Fourth Annual Midyear Topical Symposium, Health Physics Society Meeting, Louisville, Kentucky, January 28-30, 1970.
14. S. Fine - Lasers in Industry, Associated Hazards and Protection - National Safety Congress, Chicago, Illinois, October 28, 1970.
15. S. Fine - Uses and Hazards of Laser Radiation in Industry and in Atmosperic Pollution Studies - 24th AMA Clinical Convention, Boston, Massachusetts, November 30, 1970.